

SEVER INSTITUTE OF TECHNOLOGY

MASTER OF SCIENCE DEGREE

THESIS ACCEPTANCE

(To be the first page of each copy of the thesis)

DATE: April 25, 2006

STUDENT'S NAME: Erik H. Clayton

This student's thesis, entitled Frequency Correlation-based Structural Health Monitoring with Smart Wireless Sensors has been examined by the undersigned committee of three faculty members and has received full approval for acceptance in partial fulfillment of the requirements for the degree Master of Science.

APPROVAL: _____ Chairman

WASHINGTON UNIVERSITY
THE HENRY EDWIN SEVER GRADUATE SCHOOL
DEPARTMENT OF CIVIL ENGINEERING

FREQUENCY CORRELATION-BASED STRUCTURAL HEALTH
MONITORING WITH SMART WIRELESS SENSORS

by

Erik H. Clayton, B.S., E.I.T.

Prepared under the direction of Professor S.J. Dyke

A thesis presented to the Henry Edwin Sever Graduate School of
Washington University in partial fulfillment of the
requirements for the degree of

MASTER OF SCIENCE

May 2006

Saint Louis, Missouri

WASHINGTON UNIVERSITY
THE HENRY EDWIN SEVER GRADUATE SCHOOL
DEPARTMENT OF CIVIL ENGINEERING

ABSTRACT

FREQUENCY CORRELATION-BASED STRUCTURAL HEALTH
MONITORING WITH SMART WIRELESS SENSORS

by

Erik H. Clayton

ADVISOR: Professor S.J. Dyke

May 2006

Saint Louis, Missouri

The rapid development of inexpensive smart wireless sensing devices has triggered the onset of a revolutionary transformation in data acquisition and reconnaissance paradigms, the likes of which can be harnessed for vibration-based structural health monitoring (SHM). Referred to as simply a “mote”, these devices integrate a microprocessor, computational memory, and a radio transmitter into one small battery operated instrument and are often equipped with a low power MEMS technology sensor. Since the mote-sensor combination has the ability to virtually *listen*, *think*, and *talk* the development of a smart wireless sensor network for infrastructure preservation is an advantageous prospect for the vibration-based structural health monitoring community. Deploying large ensembles of motes could allow for automated feature extraction, damage identification, and coordinated response decisions to be made online through embedded adjudicatory algorithms. However, despite the promising attributes of a wireless sensor network there are limitations which need to be addressed. Recent studies have shown that streaming data over the low power radio communication links at rates sufficient for SHM results in data losses and is too power consumptive. As such, there is a need to decentralize the traditional infrastructure monitoring system concept in order to better exploit the onboard computational facilities of a mote. Hence the motivation of this work is to develop and test the efficacy of a vibration-based condition assessment algorithm which can be embedded within a wireless smart wireless sensor for structural health monitoring.

copyright by
Erik H. Clayton
2006

Ne quid nimis.

Contents

List of Tables	vii
List of Figures	viii
Acknowledgments	x
Preface	xi
1 SHM with Smart Sensor Networks	1
1.1 An Introduction to Health Monitoring	1
1.1.1 The Purported Origin of Vibration-based SHM	1
1.1.2 US Infrastructure Preservation Procedures	2
1.1.3 Vibration-based Infrastructure Health Monitoring	2
1.2 Micro-Electrical Mechanical Systems	4
1.3 Notes	5
1.4 SHM Implementing SWS/SWSN	7
1.5 Current Limitations of a SWS/SWSN	10
1.6 Overview of this Work	12
2 Global Linear System Dynamics	13
2.1 Theoretical Parameter Formulation	13
2.1.1 Single Degree of Freedom System Dynamics	13
2.1.2 Multiple Degrees of Freedom System Dynamics	16
2.2 Experimental Parameter Formulation	17
2.2.1 Spectral Analysis	17
2.2.2 Complex-curve Fitting	18
2.3 Summary	21
3 A Distributed SHM Algorithm for SWSN	22
3.1 Why Distributed SHM Algorithms?	22

3.2	Feature Correlation-based SHM	23
3.3	Damage Location Assurance Criterion	26
3.4	The Proposed Distributed SWS Framework	29
3.5	Summary	31
4	Algorithm and System Integration: Offline	32
4.1	Overview	32
4.2	A Slender Cantilever Beam	33
4.2.1	Hardware	35
4.2.2	Frequency Identification	38
4.2.3	Damage Localization	40
4.3	Five Storey Shear Building Model	42
4.3.1	Hardware	44
4.3.2	Frequency Identification	46
4.3.3	Damage Localization	48
4.4	Summary	48
5	DLAC Sensitivity Analysis	50
5.1	Motivation	50
5.1.1	Spatial Quantization	51
5.1.2	Simulation Noise Distribution	52
5.1.3	Absolute DLAC Correlation	55
5.2	Simulation Procedure	56
5.3	Generalized Parameters	57
5.4	The L_m Distance as a Sensitivity Metric	59
5.4.1	DLAC Correlation Behavior	60
5.4.2	Establishing the Success Criterion	63
5.5	Sensitivity to Spatial Quantization	64
5.6	Measurement Noise	65
5.7	Modal Truncation	69
5.8	Summary	73
6	Conclusion and Future Work	74
6.1	Conclusions	74
6.2	Future Works	76

Appendix A	Mote Developments	78
Appendix B	ADXL202E MEMS Accelerometer	82
Appendix C	Damage Simulation and its Effects on W_n	85
Appendix D	Additional Figures	87
References	89
Vita	95

List of Tables

1.1	Rytter's (1993) Classification of Damage Detection Methods [50]. . . .	3
1.2	Performance Capabilities of a Few Commercial Motes	7
4.1	Natural Frequencies (Hz): FE Model	35
4.2	Performance Specifications: Mica Series Motes [11]	35
4.3	Performance Specifications: ADXL202JE MEMS Accelerometer [1, 11]	37
4.4	Natural Frequencies Identified (Hz): Mica2 Motes	39
4.5	Natural Frequencies Identified (Hz): Wired System	39
4.6	Natural Frequencies (Hz): FE Model	44
5.1	Average L_d Value: 4 Modes	64
5.2	Average L_d Value: 5 Modes	69

List of Figures

1.1	The Advantages of a MEMS Accelerometer	5
1.2	Current Measurement Time History of Mica2 Mote [52]	10
1.3	Theoretical Mica Series Mote Radio Transceiver Bandwidth (CSMA)	11
2.1	Generalized Single Degree of Freedom Model	14
2.2	Generalized Multiple Degrees of Freedom Model	16
2.3	Levy's Curve-fitting Method with System Noise	21
3.1	Data Acquisition Configurations	23
3.2	The Principle of Correlation-based SHM	24
3.3	Frequency Change Vectors in R^3 Space	27
3.4	Correlation Comparison: $DLAC_j$ vs. C_j	28
3.5	DLAC Smart Wireless Sensor Network Framework	30
3.6	DLAC Smart Wireless Sensor Network Operation	31
4.1	Cantilever Beam Setup (not to scale)	33
4.2	Transmission Data Loss in Time History, $F_s = 100$ Hz	37
4.3	Power Spectrum of System with Damage at Location D3	38
4.4	DLAC Localization: 51 Node Model, 20% Simulated Damage, 4 Modes	41
4.5	DLAC Localization: 19 Node Model, 500% Simulated Damage	41
4.6	DLAC Localization: 215 Node Model, 10% Simulated Damage	42
4.7	Building Model Setup (not to scale)	43
4.8	TDMA Transmission Schedule Example	45
4.9	FPCF Wireless Sensor Data	46
4.10	Experimentally Identified Resonant Frequencies	47
4.11	DLAC Localization Result	48
5.1	Messina <i>et al.</i> (1996) DLAC Validation Model [38]	51
5.2	Spatial Quantization	52
5.3	Errors Attributed to Automated Frequency Extraction	53

5.4	Process Diagram: Modeling and Simulation Procedure	56
5.5	Finite Element Method and Exact ODE Solution Frequency Convergence	59
5.6	The L_d Performance Metric	60
5.7	L_d Example of Good Localization	61
5.8	L_d Example of Poor Localization	62
5.9	L_d vs. Damage Location (4 Modes)	63
5.10	DLAC Quantization Performance Noise: $M = .0625$, 4 Modes	65
5.11	DLAC Quantization Performance Noise: $M = .1250$, 4 Modes	66
5.12	DLAC Quantization Performance Noise: $M = .2500$, 4 Modes	66
5.13	DLAC Quantization Performance Noise: $M = .5000$, 4 Modes	67
5.14	DLAC Quantization Performance Noise: $M = 1.000$	67
5.15	Measurement Noise: $M = 1.000$, 20 Modes [38]	68
5.16	DLAC Truncation Performance: 15% Gaussian Noise, $M = 0.125$. .	70
5.17	DLAC Truncation Performance: 15% Gaussian Noise, $M = 0.250$. .	70
5.18	DLAC Truncation Performance: 15% Gaussian Noise, $M = 0.500$. .	71
5.19	DLAC Truncation Performance: 15% Gaussian Noise, $M = 1.000$. .	71
5.20	Modal Truncation: 15% Uniform Noise, $M = 1.000$, $D^* = 1.000$, [38]	72
A.1	Commercial Smart Wireless Sensing Units (1999–2003) [33]	79
A.2	Academic Smart Wireless Sensing Units (1998–2003) [33]	80
A.3	Academic Smart Wireless Sensing Units (2003–2005) [33]	81
B.1	Functional Block Diagram: ADXL202E MEMS Accelerometer [1] . .	83
C.1	Nonlinear ω_n Relation (SDOF)	86
D.1	Histogram of Gaussian Noise Implemented	88
D.2	Histogram of Uniform Noise Implemented	88

Acknowledgments

Drs. S. J. Dyke, C. Lu, and B. H. Koh provided the guidance required to complete this work, without their efforts this work could not have been completed. Fellow colleagues G. Xing, C. L. Fok, and O. Orjih provided technical hardware and software support during this project, without their efforts this project would have never moved from conceptual discussions to practical implementation.

Dr. A. Mita provided laboratory space, test equipment, and a test structure while hosting my summer research appointment at Keio University in 2005. Fellow colleague Y. Qian contributed greatly to the research investigations conducted in Japan.

Tom Stroebel and Lama Nachman at Intel Corporation were extremely helpful during the final months of this project.

Financial support for this investigation was provided by the United States Department of Education GAANN fellowship program and the National Science Foundation through grants CMS-0245402 and EEC-0243809.

Erik H. Clayton

Washington University in Saint Louis
May 2006

Preface

Civil infrastructure is found at virtually every inhabited place on earth. The buildings we work and live in, the dams and offshore structures that provide us with energy, and the highway and railway network of roads and bridges are all examples of civil infrastructure. Nearly every facet of our existence can be traced back to a dependence on the role these structures serve. As a result, there is a clear need to continuously maintain the function of these structures well into the future.

Chapter 1

SHM with Smart Sensor Networks

1.1 An Introduction to Health Monitoring

1.1.1 The Purported Origin of Vibration-based SHM

Infrastructural health monitoring or condition monitoring by way of a structure's global dynamic behavior is not a new concept. It has been suggested that some of the first clay potters would strike their fired clayware and listen to its tone as a way to determine if the vessel was flawed [50]. The artisan understood that any deviation from the expected norm in the tone indicated the presence of a defect in the work. This is quite an impressive discovery and an interesting point to make since the oldest known collection of pottery has been dated to as early as 10,500 BC¹ [42].

The same concept applies to other structures, and this effect is the central motivation of global vibration-based structural health monitoring. There are really only two fundamental differences between the monitoring done by ancient potters and such systems today. The mathematics behind the monitoring process are better understood, i.e. for some linear systems close-form expressions for oscillatory motion can be developed, and instead of the human ear innovative sensing devices are used to record data. Despite these changes virtually the same monitoring process is performed today.

¹Pottery found throughout the Japanese islands has been radiocarbon dated to around the 11th millennium BC, at the end of the Japanese Jomon period, and is accepted to be the oldest known set of such artifacts [58].

1.1.2 US Infrastructure Preservation Procedures

Presently in the United States structural integrity is monitored by simple techniques such as visual inspection, concrete sounding (hammer echo), dye-penetrant, and ultrasonic [24]. These condition monitoring techniques can provide strong indications of the presence of damage if tests are performed on potential damaged areas. This means that if there is no prior knowledge of damage the structure must be scrupulously examined and that the inspector is well trained in diagnosing test results which may only reveal potential symptoms of damage.

There are other limitations concerning the use of these procedures in a field environment which need to be addressed. These methods are labor intensive and time consuming, perhaps requiring both a trained field technician to perform tests and a structural engineer to interpret results. As such, inspections can become costly and this large expense is likely to effect the rate at which they are conducted. For example, bridges in the US may undergo a scheduled inspection every four years [24]. While fully constructed buildings may not be inspected until after a natural disaster occurs and damage is explicitly evident, e.g. excessive cracking or a leaning structure.

All of the aforementioned methods, aside from ultrasonic, require preliminary visual inspections to locate potential damage sites for testing [24]. Thus, these methods are most successful when all critical structural elements are exposed, in an open air environment, i.e. critical load bearing members are not obstructed by non-structural elements. In a building such a situation is unlikely. Moreover, the labor intensive manual inspection process coupled with hazardous working conditions can fatigue workers. This fatigue in turn could introduce judgement errors which may undermine safety of the structure despite the preventative measures being taken.

1.1.3 Vibration-based Infrastructure Health Monitoring

In response to limitations associated with manual inspection methods and the need to keep US infrastructure functioning, more robust monitoring alternatives are being

sought. Currently, analytical health monitoring methodologies based on the mathematics describing simple harmonic motion are being developed. These health monitoring schemes are generally classified by the extent of damage information they can extract from structural response behavior. Rytter (1993) is credited with the first of such classifications, cf. Table 1.1, [50]. Within the last two decades many

Table 1.1: Rytter’s (1993) Classification of Damage Detection Methods [50].

Category	Classification
Level I	<i>Detection</i> —a qualitative indication that damage is present
Level II	<i>Localization</i> —the probable location of damage
Level III	<i>Assessment</i> —the size of damage
Level IV	<i>Consequence</i> —the safety of the structure given a certain damage state

of these mathematical techniques have been borrowed from the aerospace industry and applied to civil infrastructure with some success. However, the transition from aerospace structures to that of civil has proven to be quite challenging for several reasons.

Civil structures are generally massive, composite systems composed of reinforced concrete, mild steel, masonry, and a slue of non-structural elements. Each of these materials exhibits a different behavior under the same sustained loading conditions and a different primary mode of failure. As such, their interaction in a structural system can be complex. Perhaps intensifying matters more, civil structures are often exposed to various uncharacterized (non-periodic) loading conditions; such as, automotive traffic, wind, and earthquakes. Composite concrete members and bolt connection “backlash” introduce a source of complex geometric system nonlinearities which are often neglected for global vibration analysis. Soil and fluid-structure interactions complicate modal parameter analysis by augmenting the structure’s boundary conditions over time; introducing a form of time dependent nonlinearity [60]. Structures can suffer from excessive fatigue cracking before global system parameters are noticeably effected [19]. This behavior can disguise damage until the structure is at a point of incipient catastrophic failure².

²This is certainly not an exhaustive list, but the discussion ends here as the author has made his point.

Despite the complexities of civil structures several global vibration-based monitoring methodologies have been developed which have been able to address some of their uncertainties. Statistically based algorithms, such as probabilistic neural networks (PNN) appear to be some of the most advantageous methodologies [16, 29]. PNN's simulate the behavior of the human brain and effectively “learn” how to distinguish damage, much like the ancient potters. As these methods continue to develop infrastructure owners and insurers will begin to fully appreciate the benefits of this type of SHM system.

To date, the greatest hurdle facing the implementation of a vibration-based SHM system is its cost. It is expensive to extract damage sensitive features from a structural response behavior with traditional tethered systems. For example, consider a monitoring paradigm based on natural frequencies. The multiplicity of low amplitude, large period oscillations of civil structures requires a high performance data acquisition system sensitive enough to accurately extract these features. These systems are expensive, which hardware alone can cost several thousands of dollars per sensor channel [33]. Moreover, to provide accurate estimates of the features to be extracted these systems often require a dense array of sensors to average the data acquired. The installation of dense sensor arrays is expensive. Wiring and conduit have been priced as much as 40 dollars per linear foot which for some applications can exceed the cost of the sensor and acquisition hardware itself [15].

1.2 Micro-Electrical Mechanical Systems

Micro-electro mechanical systems (MEMS) were developed through what is called the very large system integration (VLSI) [53]. VLSI is the process of placing thousands of electronic components onto a single silicon substrate using micro-fabrication technology [37]. MEMS integrate mechanical elements with the electronics required to operate them on a single chip [37]. As such, complete systems-on-a-chip can be developed.

MEMS technology has already shown it has much to offer the health monitoring community by developing complete ultra small, low power sensor and actuator hardware.

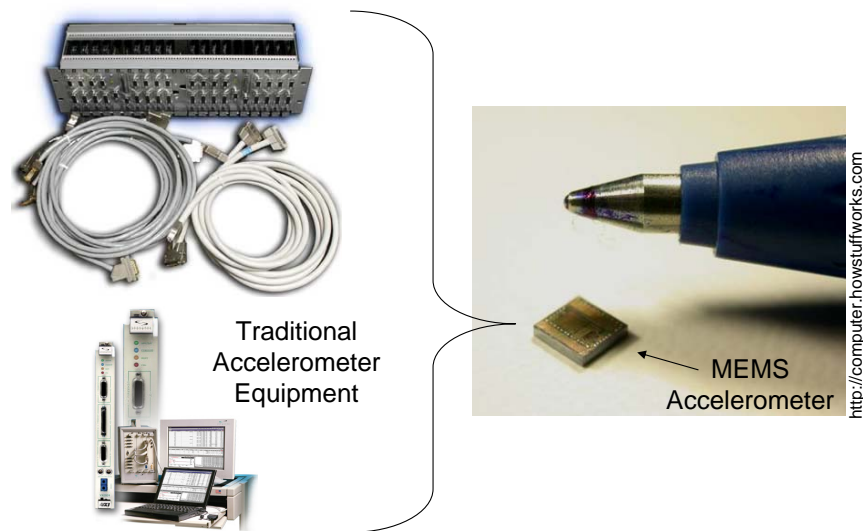


Figure 1.1: The Advantages of a MEMS Accelerometer

Consider the advantages of a MEMS accelerometer, cf. Figure 1.1. With such a device the all of the hardware required to operate and extract meaningful data from the sensing unit, e.g. signal conditioner, acquisition hub, multiplexer, analog-to-digital converter, can be combined into one ultra small device.

Needless to say, these advancements have sparked the interests of many researchers in the field of vibration-based structural health monitoring [53, 26, 33]. One of the first was Vandiver (1997) who instrumented a Patriot missile with MEMS technology sensors for SHM [20]. Since this study researchers have realized the potential of these devices and there is now a push to do more digital processing at the measurement site [26, 33, 49, 21]. Recently, remote wireless computational units have been developed to meet this demand and the result has been revolutionary, as it is now reasonable to envision wireless networks of “smart” MEMS sensors.

1.3 Motes

Motes are the building blocks of smart wireless sensor networks (SWSN). They are tiny, often battery operated devices which integrate a microprocessor, computational memory, and a radio transmitter together onto one platform. Some motes can be

configured to acquire data with an array of industry standard sensors, but they are currently being developed to encompass the breakthrough strides of MEMS technology. Coalescing these features onto one device enables motes to gather, process, and exchange data with one another in self-organized ad hoc networks. As such, the *remote* data acquisition and in-situ data processing capabilities not only give a mote its name, but also a powerful advantage over traditional wired data acquisition systems.

The first of such remote smart sensor platforms were developed at UC Berkeley under the guidance of David E. Culler³ with substantial funding from the US Defense Advanced Research Projects Agency (DARPA). DARPA is interested in the idea of deploying such devices on a potential battlefield to monitor the movement of hostile forces. Known as the “Smart Dust” project, the objective of this program is to construct a massive distributed sensor network of more than 1000 devices [13]. Major mile stones listed for the project include developing a 1 mm³ mote which can transmit data more than 1 km [14].

While several researchers in the academic community have developed smart wireless sensor prototypes they are not readily accessible to those researching in SHM⁴. On the other hand, off-the-shelf commercially developed motes are easier to acquire. In addition, commercial mass production of these systems has reduced their cost. As a result, mote systems have become an attractive research topic in networked data acquisition and distributed data processing for vibration-based SHM. To date two of the most prominent commercial developers of mote systems have been Crossbow Technology, with its Mica series, and Intel Corporation, with its iMote series. A brief overview of the performance capabilities of these motes is presented in Table 1.2.

³Presently Culler with many of his former student have founded their own design, develop, and deployment sensor network company, Arch Rock, Inc. [2]. With investors such as New Enterprise Associates, Shasta Ventures and Intel Capital it will be interesting to see how this venture progresses in the near future [2].

⁴See Appendix A for tables documenting these developments.

Table 1.2: Performance Capabilities of a Few Commercial Motes

	Mica2 (2003)	MicaZ (2005)	iMote1 (2003)	iMote2 (2006)
Processor	ATmega128L	ATmega128L	ARM7TDMI	PXA27x
Processor Speed	8 MHz	8 MHz	12 MHz	416 MHz
Processor Bus Size	8-bit	8-bit	32-bit	32-bit
Program Memory	128 kB	128 kB	—	32 MB
Data Memory	4 kB	4 kB	64 kB	256 kB
Flash Memory	512 kB	512 kB	512 kB	32 MB
Radio	CC1000	CC2420	ZV4002	CC2420
Max Data Tx Rate	38.4 kbps	250 kbps	720 kbps	250 kbps
Accelerometer	ADXL202JE	ADXL202JE	ADXL202JE	LIS3L02DQ

1.4 SHM Implementing SWS/SWSN

One of the first efforts to perform vibration-based SHM with a smart wireless sensor may have been Mitchell *et al.* (1999) [40]. Here the architecture for a multi-chip-module (MCM) smart wireless sensor for SHM was presented. What distinguishes this work from others around the same time, namely Pines and Lovell (1998), is that new hardware was developed to perform digital signal processing before wireless transmission [46]. In this study smart wireless sensors (SWS) were developed to pre-process multiple channels of analog data acquired from non-MEMS piezoelectric (PVDF) patches. Essentially this consisted of signal conditioning, multiplexing, and analog-to-digital conversion prior to transmission. Streaming digital measurements were cached and buffered appropriately for wireless transmission to a central data acquisition point via a 900 MHz spread spectrum transceiver. To validate the SWS performance a damage detection experiment was conducted with cantilever beam test structure. The N4SID subspace identification SHM technique was implemented. The structure was excited with a chirp signal (4–100 Hz) using a piezoelectric (PZT) actuator patch and damage was simulated by mass change. State space models were computed from test data acquired wirelessly at a base station computer. Shifts in natural frequencies and phasing could be realized for the damage imposed. Data rates of only 50 kbps could be obtained, as such streaming time histories of digital accelerometer readings proved to be problematic. The 2.6–16 V power draw of the

transceiver alone raised questions concerning the viability of the system due to power requirements.

More recent studies with Mica generation motes indicate that complete time history records may be transmitted wirelessly at sampling rates sufficient for accurate spectrum characterization of civil structures. Xu *et al.* (2004) focused on reliably acquiring and transmitting structural response time histories with a custom built, high quality “vibration card” and Mica2 motes [59]. To mitigate wireless transmission data losses attributed to the 38.4 kbps bandwidth of the Mica2’s radio, retransmission and compression schemes were investigated. The result was the development of a wireless structural data extraction network named Wisden, a system which is suitable for centralized data processing. To validate the work a ten mote system was deployed on a ceiling truss structure and 20 seconds of response time history were recorded at 50 Hz and then transmitted to a central base station within a five minute period. In this study no consideration was given to the development of a SHM system.

Later Caffrey *et al.* (2004) laid out the framework for a distributed monitoring scheme to be implemented on the Wisden system [4]. They focused on the interplay between networked sensing and the monitoring paradigm, a two-phase, embedded distributed algorithm was envisioned for the network. At phase one motes would acquire response data autonomously and calculate power spectrums onboard. Natural frequencies as well as their amplitudes would be extracted from the power spectrums at during this phase. At phase two, amplitude data would be transmitted to centralized data station and coalesced to determine qualitative vibrational mode shapes. No experimental work was completed to actually test the feasibility of onboard feature extraction and parameter calculations. However a numerical simulation of the embedded algorithm was completed using the ASCE Benchmark Health Monitoring Structure and promising results were obtained.

Paek *et al.* (2005) continued the Wisden research making several enhancements system research and development. For this study modifications were made to the Wisden system which included increasing the sampling frequency to 200 Hz and modifying the data compression scheme to prevent unintended filtering [44]. Mica2 motes were replaced with newer MicaZ motes which incorporate the ZigBee (IEEE 802.15.4) radio technology. Marketed as low power alternative to the Bluetooth specification,

the Zigbee specification offers a nominal theoretical bandwidth of more than 6 times that of Mica2 generation radios. The same ceiling truss model was used as the experimental test bed and the modified Wisden system was integrated onto a 14 mote system. A 40 second response time history was recorded and transmitted to a central base station within a five minute period. A validation experiment was performed and good agreement was found between structural response data gathered from a Wisden sensor node and a traditional wired sensor in both the time and frequency domains. This study concluded with a side-by-side performance evaluation of Mica2 and MicaZ motes. By simply implementing the MicaZ mote platform both transmission latency and data loss were minimized due to the enhanced radio bandwidth. However, excessive power consumption is a problem.

In 2006 Discenzo *et al.* developed a novel energy harvesting device that can be used to power a mote [15]. In a collaborative program between Rockwell Automation, Inc. and BP's Chief Technology Office, tiny tuned piezo-electric oscillators which operate in a magnetic flux were shown to produce enough power to fully operate a mote. To test the device two smart wireless sensors equipped with the developed energy harvester were attached to an oil pump on BP's Loch Rannoch petroleum supertanker. One of the SWS was deployed with an internal battery which would be recharged by the energy generator, another was deployed without batteries, fully dependent on performance of the energy scavenging device. SWS were configured to operate periodically. When awake, each mote was programmed to acquire a 1 second time history from a single axis accelerometer at a sampling rate of 1 kHz. Analog-to-digital conversion was completed onboard each mote with 12-bit resolution before being transmitted to a personal desktop assistant (PDA) where further data analysis was post-processed.

For comprehensive literature reviews of vibration-based SHM implementing smart wireless sensors the reader may consult Lynch and Loh (2006) and Spencer *et al.* (2005) [33, 26].

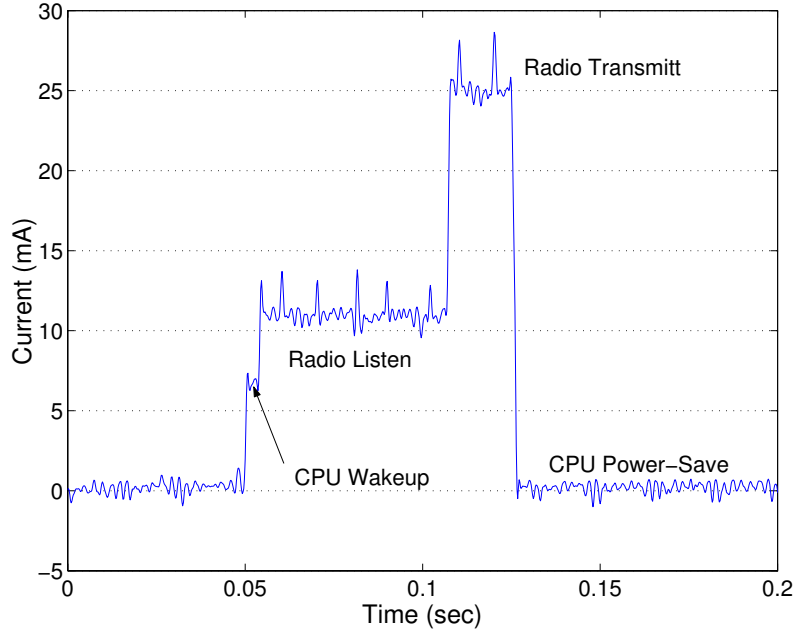


Figure 1.2: Current Measurement Time History of Mica2 Mote [52]

1.5 Current Limitations of a SWS/SWSN

Smart wireless sensing technology does have limitations which need to be addressed when considering its use for structural health monitoring. One rather obvious restriction to these systems, are their power source lifetime. Though impressive advancements have been made to develop vibration-based energy scavenging devices, these mechanisms do not appear to be well suited for implementation with civil structures [15]. In Discenzo and company's (2006) study it was fortuitous that the object instrumented was an electric pump. Such a mechanical system operates at more or less one constant frequency, so the energy generating oscillator was tuned to this energy rich frequency [15]. Civil structures are subjected to a variety of non-periodic excitations and tend to have low amplitude, long period oscillations.

Consider the amount of current consumed as a Mica2 mote performs various operations, cf. Figure 1.2 [52]. It is immediately clear that data transmission is the most current consumptive operation. In this case, what is shown in Figure 1.2 is the amount of current consumed to transmit a single radio message at full power [52].

Number of Motes	Sampling Frequency (Hz)					
		25	50	75	100	200
	1	7.2 kbps	14.4 kbps	21.6 kbps	28.8 kbps	57.6 kbps
	2	14.4 kbps	28.8 kbps	43.2 kbps	57.6 kbps	115.2 kbps
	3	21.6 kbps	43.2 kbps	64.8 kbps	86.4 kbps	172.8 kbps
	4	28.8 kbps	57.6 kbps	86.4 kbps	115.2 kbps	230.4 kbps

Mica2

MicaZ

Figure 1.3: Theoretical Mica Series Mote Radio Transceiver Bandwidth (CSMA)

When considering the relatively small amounts of current required to drive the microprocessor, ≈ 8 mA, and the MEMS accelerometer, ≤ 15 μ A, on the Mica2 mote it makes sense to avoid prolonged use of the radio transceiver [11, 1].

Another limitation of smart wireless sensors is the bandwidth of the low power radio transceiver⁵ implemented. As a result of limited radio bandwidth, data is often lost during transmissions. Consider the theoretical bandwidths required to transmit synchronized data streams simultaneously, cf. Figure 1.3. Note the feasible data rates which the Mica2 and MicaZ motes can theoretically support (Mica2 is shaded).

For the Mica2 mote the fastest rate at which synchronized data can be reliably transmitted in realtime is 50 Hz. As such, to prevent aliasing a sensor can only gather reliable data within a range of 0–25 Hz. This bandwidth is much less than the typical 100–200 Hz minimum bandwidth desired for extracting features from civil structural response behavior with sufficient resolution. Moreover, only two Mica2 motes can be supported simultaneously at this data rate. Recall, the MicaZ mote radio functions with the IEEE 802.15.4 protocol, it is slightly more power efficient consuming only 19.7 mA during data transmissions and has a much greater bandwidth than the Mica2 radio. Despite the improvements offered by the new wireless transmission protocol, MicaZ motes are still limited by both its radio bandwidth and power consumption.

⁵Relative to high power transmissions such as AM and FM radio, not relative to other sensor components onboard the mote.

1.6 Overview of this Work

Under existing vibration-based SHM paradigms, which are developed around centralized data processing, it is unlikely that a remote wireless sensor will prove to be an advantageous alternative. If vibration-based structural health monitoring paradigms are shifted to exploit the onboard, low power processing facilities of smart wireless sensors, then several key improvements could be made. Namely, a smart wireless sensor network used for vibration-based health monitoring may be able to:

- *Curtail sensor deployment costs*
- *Curtail data acquisition hardware costs*
- *Increase sensor coverage*
- *Increase monitoring fidelity*
- *Increase monitoring adaptability*

It is now the work of the engineer to design health monitoring systems which can function within the limitations of these new devices. As such, this work focuses on developing a distributed-process, vibration-based health monitoring paradigm for implementation on a smart wireless sensor platform (Chapter 3). Then to validate the algorithm examined in this study, two proof-of-concept experiments are discussed using unmodified commercially produced nodes equipped with MEMS accelerometers (Chapter 4.) Finally, this work concludes with a numerical sensitivity analysis of the proposed feature correlation metric implemented within the developed SHM algorithm (Chapter 5). Conclusions and future work are discussed in Chapter 6.

Chapter 2

Global Linear System Dynamics

In this chapter the theoretical basis behind global vibration-based structural health monitoring is presented. From this understanding one method by which the modal parameters of a structure can be obtained via experimental response time history records is introduced.

2.1 Theoretical Parameter Formulation

Consider a structural system with mass, damping, and stiffness which has been excited by an impulse and is presently undergoing free oscillatory motion. If the materials strain in a linear elastic manner and dissipate energy at a rate proportional to velocity then the behavior of the system will adhere to the laws of simple harmonic motion. As such, a close form expression can be derived.

2.1.1 Single Degree of Freedom System Dynamics

Take for example the generalized single degree of freedom lumped parameter system illustrated in Figure 2.1. From Newton's Second Law, which states forces is equal to mass times the derivative of velocity, the following equation of motion can be written. Without loss of generality consider the linear homogeneous second-order ordinary differential equation of motion for an arbitrary single degree-of-freedom structure, cf.

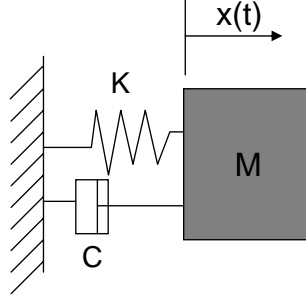


Figure 2.1: Generalized Single Degree of Freedom Model

Equation 2.1.

$$m\ddot{x} + c\dot{x} + kx = 0 \quad (2.1)$$

where m , c , and k correspond to a system's mass, damping, and stiffness, respectively. Since the system is unforced, i.e. undergoing free oscillatory motion, initial conditions $\dot{x}_0 = \dot{x}(0)$ and $x_0 = x(0)$ are defined.

Now Equation 2.1 is manipulated into standard form

$$\ddot{x} + \frac{c}{m}\dot{x} + \frac{k}{m}x = 0 \quad (2.2)$$

Let $\frac{k}{m} = \omega_n^2$, where ω_n is known as the natural frequency of the system. If the system is proportionally damped then $\frac{c}{m} = 2\zeta\omega_n$, where ζ is the fraction of critical damping. Making these substitutions into Equation 2.2 becomes

$$\ddot{x} + 2\zeta\omega_n\dot{x} + \omega_n^2x = 0 \quad (2.3)$$

and a solution to this ordinary differential equation is found by assumption.

As such, assume a solution of the following form

$$x(t) = e^{st} \quad (2.4)$$

and substitute this expression into Equation 2.3. The result is a quadratic equation in s .

$$(s^2 + 2\zeta\omega_ns + \omega_n^2)e^{st} = 0 \quad (2.5)$$

Note $e^{st} \neq 0$, and so the solutions of s are readily accessible by way of the quadratic formula.

$$s_{1,2} = \frac{-2\zeta\omega_n \pm \sqrt{4\zeta^2\omega_n^2 - 4\omega_n^2}}{2} \quad (2.6)$$

With further simplification the roots of Equation 2.6 are reduced to

$$s_{1,2} = -\zeta\omega_n \pm i\omega_n\sqrt{1 - \zeta^2} \quad (2.7)$$

where $\omega_n\sqrt{1 - \zeta^2}$ is referred to as the damped natural frequency and simply denoted as ω_{nd} .

The general solution of Equation 2.1 must encompass both roots of s .

$$x(t) = A_1e^{st} + A_2e^{st} \quad (2.8)$$

$$x(t) = e^{-\zeta\omega_n t}(A_1e^{i\omega_{nd}t} + A_2e^{-i\omega_{nd}t}) \quad (2.9)$$

Recalling Euler's Identity

$$re^{i\theta} = r(\cos \theta + i\sin \theta) \quad (2.10)$$

the following expressions for sine and cosine can be formed

$$\cos \theta = \frac{e^{i\theta} + e^{-i\theta}}{2} \quad (2.11)$$

$$\sin \theta = \frac{e^{i\theta} - e^{-i\theta}}{2i} \quad (2.12)$$

and substituted into Equation 2.9. The resulting expression can now be written in terms of two unknown coefficients A and B :

$$x(t) = e^{-\zeta\omega_n t}(A \cos \omega_{nd}t + B \sin \omega_{nd}t). \quad (2.13)$$

By instating the initial conditions unknown coefficients A and B are determined and a solution to the homogeneous differential equation of motion is obtained. A general form of the solution is presented in Equation 2.14.

$$x(t) = e^{-\zeta\omega_n t}\left(x_0 \cos \omega_{nd}t + \frac{\dot{x}_0 + \zeta\omega_n x_0}{\omega_{nd}} \sin \omega_{nd}t\right) \quad (2.14)$$

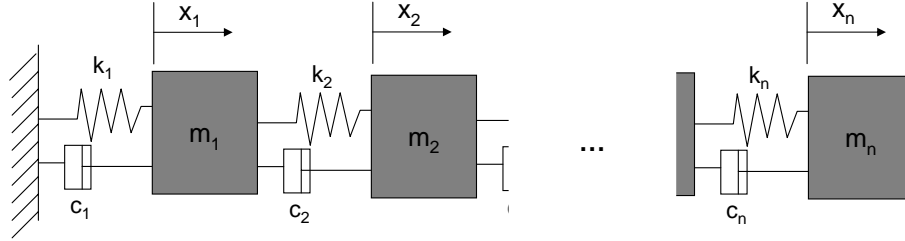


Figure 2.2: Generalized Multiple Degrees of Freedom Model

It is clear from the intrinsic equation of motion, cf. Equation 2.1, that the system modal parameters, i.e. ω_n and ζ , are completely dependent on the system's mass, damping, and stiffness characteristics¹. Consequentially, any variation in the system modal parameters must be from a change these system characteristics.

2.1.2 Multiple Degrees of Freedom System Dynamics

Now consider the generalized multiple-degree-of-freedom system shown in Figure 2.2. Again using Newtonian mechanics the same second order homogeneous differential equation of motion as that of a single degree-of-freedom system can be written only now in a matrix form, cf. Equation 2.15.

$$[\mathbf{M}]\{\ddot{x}\} + [\mathbf{C}]\{\dot{x}\} + [\mathbf{K}]\{x\} = \{0\} \quad (2.15)$$

Equation 2.15 consists of n linearly dependent equations of motion. If a similarity transform is used the expressions can be decoupled into n linearly independent equations. As such, the single degree-of-freedom solution procedure is valid for each of the decoupled equations.

Interestingly, another modal parameter can be obtained from the multiple degree-of-freedom system equations. In addition to the natural frequencies (ω_n) and damping ratios (ζ), mode shapes (ϕ) can be obtained. Mode shapes describe spatial characteristics of each mode of vibration and are often a useful parameter worth observing for

¹It is assumed the boundary conditions are rigid and do not change over time.

vibration-based SHM. Here again the system modal parameters are fully dependent on the system's mass, damping, and stiffness characteristics.

2.2 Experimental Parameter Formulation

When a global vibration-based monitoring scheme is implemented often the actual system characteristics are not known *a priori* and must be measured. This is usually done by instrumenting a structure with sensors which measure and record the dynamic response, $x(t)$, derived in the previous section. As such, these response time histories can then be analyzed a number of different ways to extract the system's modal parameters. In this thesis a frequency domain analysis technique known generally as power spectrum analysis is implemented since it lends itself well to a distributed autonomous health monitoring scheme. (To be discussed in Chapter 3.)

The first spectral estimate of a data time series is credited to Sir Aurthur Schuster in 1898 [51]. In his work titled, "On the Hidden Periodicities of a Supposed 28 Day Cycle" he characterized the emergence of sunspots by developing a new mathematical tool for tracking the frequency of the occurrences [51]. He called this tool the *periodogram*. Since then his work has been realized by others as a way to characterize all types of cyclical behavior. The processes by which frequency analysis is presently conducted today is now recapitulated.

2.2.1 Spectral Analysis

Typically the responses of a system are acquired with accelerometers. As such, acceleration response time histories, i.e. $\ddot{x}(t)$ not $x(t)$, are analyzed to extract modal parameters which are then used in a vibration-based SHM technique to make assessments concerning the safety of a structure. The reader should note that this is acceptable since the harmonic acceleration response at a given frequency, $\ddot{x}(t)$, only differs from the displacement, $x(t)$, shown in Equation 2.14 by a scaling parameter. As such, useful modal information may still be extracted from this data.

Consider the Discrete Fourier Series Transform of an N -point sample of the periodic continuous function, $a(t)$, at sampling frequency of f_s .

$$A_k = \sum_{j=1}^{N-1} a_j e^{i2\pi jk/N} \quad (2.16)$$

where $k = 0, 1, 2, \dots, (N/2 - 1)$.

The periodogram estimate of the power spectrum is defined at $N/2 + 1$ frequencies as

$$P(f_k) = \frac{1}{N^2} [|A_k|^2 + |A_{N-k}|^2] \quad (2.17)$$

for $k = 0, 1, 2, \dots, (N/2 - 1)$. However, f_k is only defined for the zero and positive frequencies

$$f_k = \frac{k}{Nf_s} \quad (2.18)$$

for $k = 0, 1, 2, \dots, (N/2)$. High levels of power in a particular frequency bands, f_k , provide good indications of structural resonant frequencies. Mode shapes may also be qualitatively defined by using this power spectrum method, although there are better methods by which one can obtain these features.

2.2.2 Complex-curve Fitting

Often mathematical methods are used to automatically extract natural frequencies from power spectrums. In 1959 E.C. Levy presented a novel complex-curve fitting technique to extract features from system transfer functions [30]. Based on the minimization of the weighted sum of the squares of the errors between the magnitude of the actual function and a polynomial, $H(i\omega)$, this numerical method can also be used to automatically pick the peaks of a power spectrum.

Levy's technique, which determines the unknown coefficients of a fractional polynomial efficiently, and can be summarized in the following steps. Consider the polynomial, $H(i\omega)$,

$$H(i\omega) = \frac{B_0 + B_1(i\omega) + B_2(i\omega)^2 + B_3(i\omega)^3 + \dots}{A_0 + A_1(i\omega) + A_2(i\omega)^2 + A_3(i\omega)^3 + \dots} \quad (2.19)$$

which will be fit to the experimental function, $F(i\omega)$. However, for the following derivation consider the following alternative forms of $H(i\omega)$

$$H(i\omega) = \frac{(B_0 - B_2\omega^2 + B_4\omega^4 - \dots) + i\omega(B_1 - B_3\omega^2 + B_5\omega^4 - \dots)}{(A_0 - A_2\omega^2 + A_4\omega^4 - \dots) + i\omega(A_1 - A_3\omega^2 + A_5\omega^4 - \dots)} \quad (2.20)$$

and

$$H(i\omega) = \frac{N(\omega)}{D(\omega)}. \quad (2.21)$$

$F(i\omega)$ can be represented as follows,

$$F(i\omega) = R(\omega) + iI(\omega) \quad (2.22)$$

where, $R(\omega)$ and $I(\omega)$ correspond to the real and imaginary parts of $F(i\omega)$, respectively.

The numerical difference between the two functions can be calculated as,

$$\epsilon(\omega) = F(i\omega) - H(i\omega) = F(i\omega) - \frac{N(\omega)}{D(\omega)} \quad (2.23)$$

and is known as the error in fitting.

Multiplying both sides of Equation 2.23 by $D(\omega)$:

$$D(\omega)\epsilon(\omega) = D(\omega)F(i\omega) - N(\omega). \quad (2.24)$$

Realizing that $D(\omega)F(i\omega) - N(\omega)$ is a function with both real and imaginary parts the expression can be separated as follows,

$$D(\omega)\epsilon(\omega) = a(\omega) + ib(\omega) \quad (2.25)$$

where $a(\omega)$ and $b(\omega)$ are functions of ω and the unknown coefficients B_i and A_i . The magnitude of this function is

$$|D(\omega)\epsilon(\omega)| = |a(\omega) + ib(\omega)|. \quad (2.26)$$

So then, at any particular frequency, ω_k

$$|D(\omega_k)\epsilon(\omega_k)|^2 = a^2(\omega_k) + b^2(\omega_k) \quad (2.27)$$

As such, an error function, E , can then be defined as,

$$E = \sum_{k=0}^{f_s/2} [a^2(\omega_k) + b^2(\omega_k)] \quad (2.28)$$

and summed over the frequency range of the function. (Which for a discrete power spectrum is $f_s/2$.) The error function, E , is then minimized to determine the best polynomial coefficients B_i and A_i . The rest of the procedure consists of a series of linear transformations by which this can be evaluation can be efficiently conducted.

To implement this method the user needs to be able to determine the order of both the numerator and denominator polynomials of $H(i\omega)$ *a priori*. As such, a control systems approach could be used. The order of denominator polynomial of $H(i\omega)$ is proportional to the number of singularities, or resonant frequencies, to be captured by the fitting technique. Similarly, the numerator of $H(i\omega)$ relates to the number of zeros, anti-resonances, to be captured. The roots of the denominator polynomial are complex conjugate pairs that have imaginary parts corresponding to natural frequencies of the system.

Special consideration needs to be taken if the system does not have a finite zero frequency gain, i.e. a pole at the origin ($A_0 = 0$). In this situation the function can be modified by a $(i\omega)^n$ factor, where n is large enough to reduce the zero frequency magnitude. Most civil structures, with respect to system dynamics, exhibit global asymptotic stability, as such the occurrence of this situation is not of concern in this application.

Not only is Levy's method computationally efficient, but it is robust to error introduced by noise. Qualitatively consider the noisy power spectrum of a single degree-of-freedom system in Figure 2.3. Clearly the large amplitude peak at 25 Hz is the natural frequency of the system. Notice how well Levy's function fits the data despite a mean 10 db noise floor.

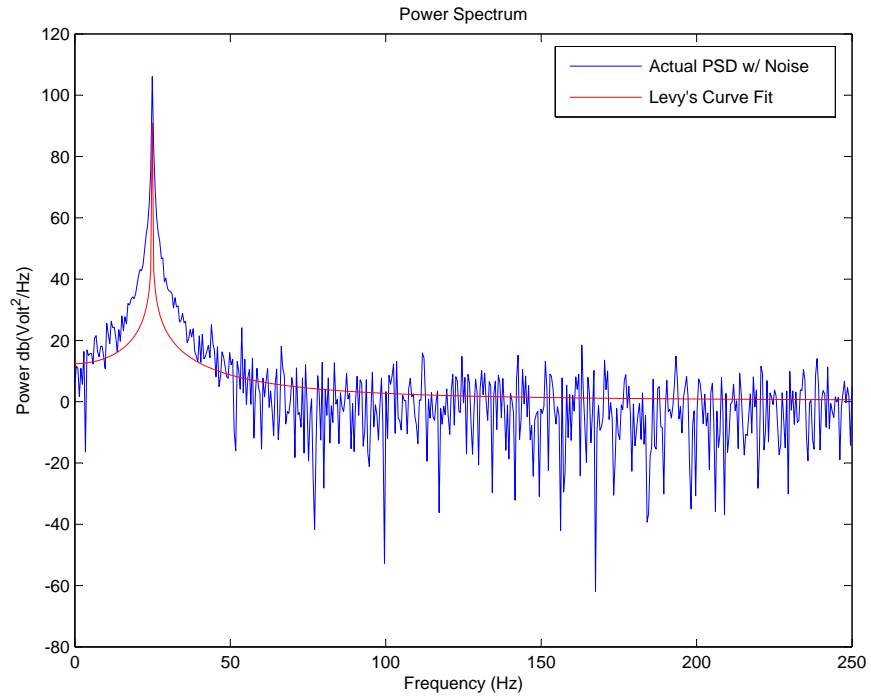


Figure 2.3: Levy's Curve-fitting Method with System Noise

2.3 Summary

In this chapter the theoretical and experimental basis of vibration-based structural health monitoring have been presented. A novel automated frequency extraction algorithm developed by Levy was discussed and shown to effectively locate a natural frequency in spite of noise. The beauty of this method is that it is not computationally intensive and could be conducted onboard a mote system as part of an embedded health monitoring algorithm.

Chapter 3

A Distributed SHM Algorithm for SWSN

In this chapter a structural health monitoring monitoring strategy is developed in collaboration with for needs of a distributed process data acquisition system.

3.1 Why Distributed SHM Algorithms?

The literature review in Chapter 1 indicates that the potential of vibration-based SHM coupled with smart wireless sensors has not yet been fully appreciated. Consider Figure 3.1, which illustrates the transmission paths of both a smart wireless sensor network and a group of smart wireless sensors. To date, SWSs and SWSNs have been configured in civil engineering applications to operate in a fashion consistent to that of a centralized data acquisition system. While complex routing and compression algorithms have been embedded on motes to increase transmission reliability, the end objective has been to send all data to one centralized collection center for post-processing [59, 44, 4].

Despite new advancements in wireless radio transmitters, better radios themselves do not appear to be able to address the demands of a dense wireless sensor network as envisioned for health monitoring. That is to say that transmission power consumption, radio bandwidth, and latency attributed to data compression schemes will continue to stand in the way of the development and implementation of a full-scale SWSN for centralized SHM.

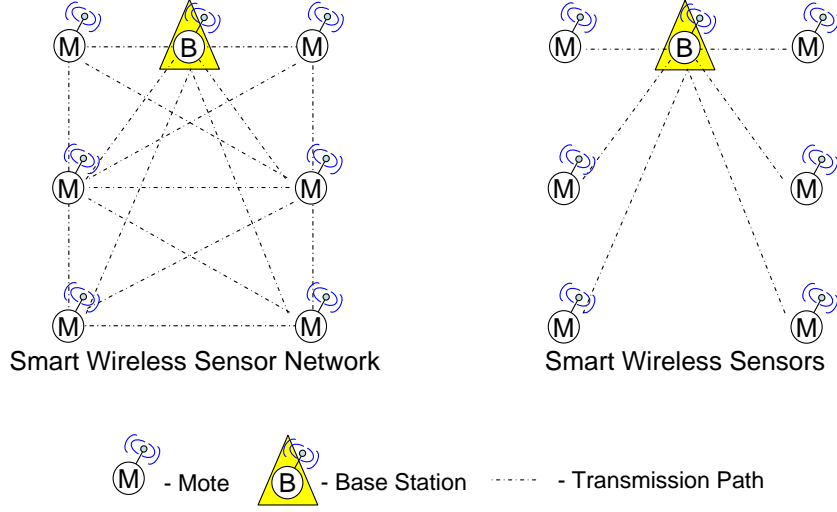


Figure 3.1: Data Acquisition Configurations

Clearly, the idea of using a dense SWSN that can exchange reduced sets of data to increase the global sensitivity of an SHM method would be advantageous. As such, distributed SHM algorithms which extract meaningful features from response data without multiple channels of data need to be embedded on SWS. In response to this limitation placed on data transmission a decentralized smart wireless sensor paradigm for vibration-based SHM is proposed here.

3.2 Feature Correlation-based SHM

Feature correlation-based monitoring techniques essentially function by comparing the characteristics a numerical model to those of the actual structure. In general, these methods are implemented according to the following concept. Mathematical features are extracted from measured structural response behavior and compared to a database of features extracted from response behavior generated by a numerical model of the structure. The numerical model is damaged in various ways to simulate all, or nearly all, of the likely damage scenarios. A strong correlation between a set of observed structural features and those features generated by way of a numerical model can indicate the actual structure's condition is similar to that of the model's,

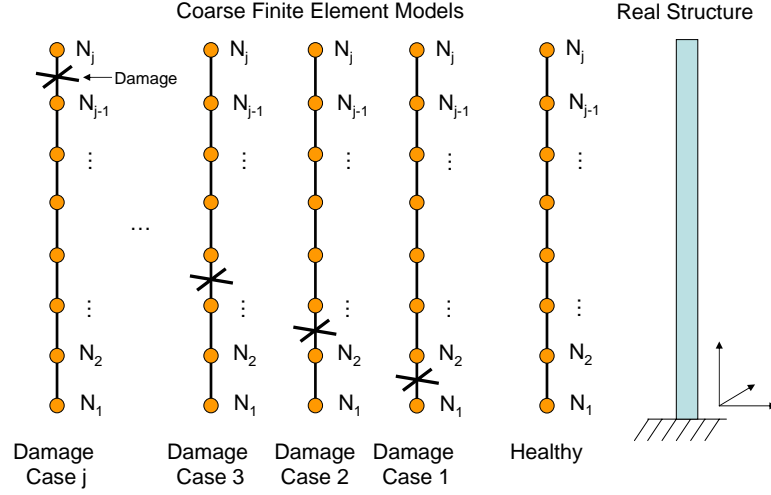


Figure 3.2: The Principle of Correlation-based SHM

i.e. one can assert the actual structure is damaged in the same way the model is damaged.

For example, consider Figure 3.2. Here the real structure is a vertical cantilever beam. Notice the “healthy” finite element model depicted. The healthy numerical model is used to generate and subsequently simulate all of the possible damage scenarios. (Several of which have been illustrated along side the healthy model.) The damage models are then used to generate mathematical features which are correlated to those extracted from the real structure. If a strong correlation exists between a particular damage model and the real structure, damage is identified and located on the actual structure according to the damage case simulated in that model.

The success of a correlation-based method hinges on both the correlation technique and the feature one selects for monitoring. For example, it has been suggested that Ritz vectors are a feature which is highly sensitive to even low levels of damage [29]. As such, selecting this feature to monitor may help to more precisely distinguish damage cases apart from one another and enhance the performance of the correlation technique used. However there is often a cost associated with extracting such sensitive features. Stacked mode shapes have been shown to be an extremely good indicator for damage detection and localization [28]. However, multiple channels of data are required to be processed simultaneously to accurately obtain mode shapes.

As previously discussed, acquiring and transmitting multiple channels of data with a SWS is considered to be a permanent hurdle.

Autoregressive moving average coefficients have been widely researched for use as correlation features as an alternative to using natural frequencies [53, 34]. In 1995 Lew used transfer function coefficients as features to diagnose damage [31]. Surely the first feature ever monitored for damage detection and by far the most common is a structure's natural frequencies. There are a variety of features which have successfully tested in previous studies and are available for use.

Cawley and Adams' (1979) presented one of the first types of correlation techniques to be used for damage localization [5, 38]. This rather crude technique compared ratios of consecutive natural frequencies obtained experimentally with those obtained using a numerical model [5]. Since then more sophisticated methods have been introduced which aim to reduce both the database size and the computational intensity, yet heighten localization accuracy. Lew (1995) presented the inner product vector as a correlation method [31]. Using the inner product as a correlation metric simple and is now a commonly used technique.

The drawback to a correlation-based technique is that nearly all of the possible damage cases need to be generated in order to reliably detect and localize damage. If multiple damage scenarios are considered the database of damage cases can become immense and database generation becomes computationally intensive. To circumvent this problem in the past researchers have used genetic algorithms or statistical-based recognition methods [28, 39]. These methods are seen as more or less the precursors to more advanced correlation-based techniques which entail artificial or probabilistic neural networks (P/ANN). These networks are the most recent of the monitoring techniques to be developed and they function by training themselves to associate damaged features to certain sets of prescribed outcomes [29, 7, 48]. Considering all of the uncertainties associated with vibration-based health monitoring these P/ANN

methods appear to be one of the best options for future studies¹. However, several feature correlation-based health monitoring schemes appear to be well suited for distributed process smart wireless sensor networks².

Presently commercial motes are equipped with computational processing abilities that limit the features that can be extracted onboard. Since computationally efficient frequency extraction programs³ are readily available, natural frequencies were selected as the correlation feature for this work.

3.3 Damage Location Assurance Criterion

In this study the Damage Location Assurance Criterion (DLAC) correlation method developed by Messina *et al.* (1996) is utilized [38]. The proposed method was developed from the Modal Assurance Criterion (MAC). A MAC value measures the extent of linear correlation between an experimental and analytical mode shape and is typically used for validating the fidelity of an analytical model, and as such the metric is very similar the inner product vector operation. In their work Messina *et al.* show that the MAC concept can be extended damage localization by comparing natural frequency characteristics of a model with the actual structure.

The DLAC metric is a measure of correlation between a vector of experimental natural frequency change ratios with a vector of analytical natural frequency change ratios, cf. Equation 3.1.

$$DLAC_j = \frac{(\{\Delta\omega\} \bullet \{\delta\omega_j\})^2}{|\{\Delta\omega\}|^2 |\{\delta\omega_j\}|^2} \quad (3.1)$$

where the *observed* frequency change vector is defined as

$$\{\Delta\omega\} = \{\Delta\omega_1, \Delta\omega_2, \Delta\omega_3, \dots, \Delta\omega_n\} \quad (3.2)$$

¹Refer to Chapter 1.

²Doebling *et al* (1997) and Sohn *et al* (2004) offer a comprehensive reviews of the history of SHM development as well as information about numerous methodologies which have been developed to date [17, 53].

³Refer to Chapter 2

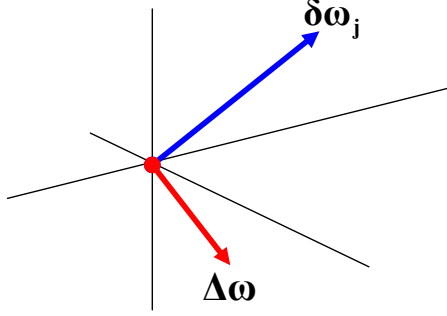


Figure 3.3: Frequency Change Vectors in \mathbb{R}^3 Space

and the *hypothesis* frequency change vector is defined for the j^{th} location as

$$\{\delta\omega_j\} = \{\delta\omega_{1j}, \delta\omega_{2j}, \delta\omega_{3j}, \dots, \delta\omega_{nj}\} \quad (3.3)$$

hence, $\{\Delta\omega\}$ and $\{\delta\omega_j\}$ are two vectors of dimension n , c.f. Figure 3.3.

Note that both $\{\Delta\omega\}$ and $\{\delta\omega_j\}$ vectors which are normalized with respect to the structure's healthy frequencies, cf. Equation 3.4.

$$\Delta\omega_i = \frac{\omega_{i,\text{observe}} - \omega_{i,\text{health}}}{\omega_{i,\text{health}}} \quad (3.4)$$

Normalizing these features in this fashion equally weights all modes of the frequency change vector and reduces bias introduced from higher modes [38].

For comparison the inner product vector correlation metric, C_j is also developed.

$$C_j = \frac{\{\Delta\omega\} \bullet \{\delta\omega_j\}}{|\{\Delta\omega\}| |\{\delta\omega_j\}|} \quad (3.5)$$

where, $C_j = \cos \theta$, $-1 \leq C_j \leq 1$, and $\theta = \angle[\{\Delta\omega\}, \{\delta\omega_j\}]$.

Consider the illustrative example comparing the performance of the DLAC method versus that of the inner product correlation in Figure 3.4. In this case the both the DLAC and inner product, C_j , correlations approach unity at the actual damage location. The effect of squaring both the numerator and denominator of the inner

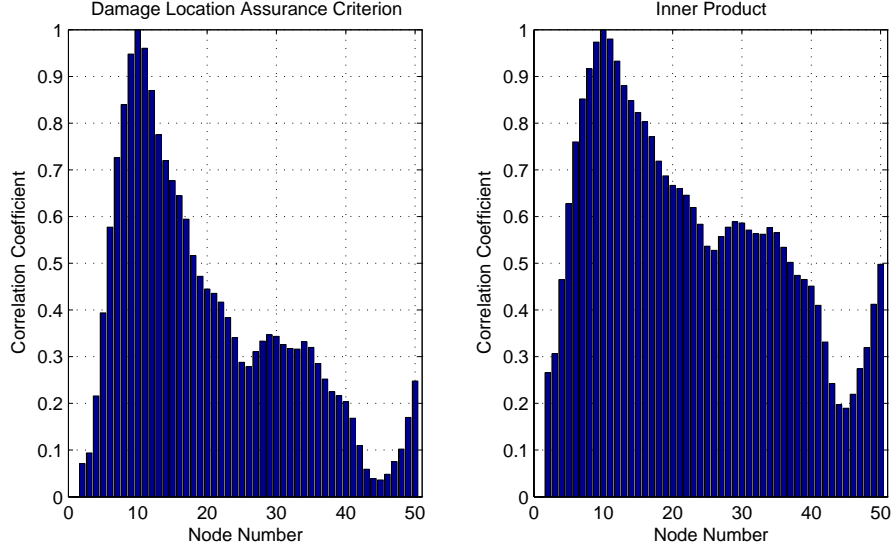


Figure 3.4: Correlation Comparison: $DLAC_j$ vs. C_j

product yields results with less noise, e.g. the area of the inner product bar plot is 28.3 and the area of the DLAC bar plot is 18.7 (51 Node Model, O:125%, H:110%).

Only single damage scenarios will be considered in this study to prevent the technique from becoming too computationally intensive for operation on currently commercially available mote hardware. It is important to note that Equation 3.1 can only be used to detect single damage occurrences, more complex methodologies must be employed to localize damage in structures suffering from multiple damages. Contursi *et al.* (1998) developed the Multiple Damage Location Assurance Criterion (MDLAC) based on the DLAC metric. However the discussion ends here as the scope of this study is limited only to single damage scenarios.

Often numerical identification models are dynamically tuned in order to facilitate accurate damage recognition and localization. For some correlation-based algorithms tuning, or updating, the numerical model so that it will more accurately depict the response of the structure may also reduce the number of calculations required for convergence. While it is common for numerical models of aerospace and mechanical structures to be dynamically tuned with experimental modal analysis results, this is

not common practice for civil structural models⁴. As such, in the models used for the DLAC correlation metric will not be updated.

A notable benefit of the DLAC metric is that the magnitude of damage simulated in the suite of hypotheses vectors does not significantly affect the results of damage localization. The sensitivity of the DLAC method to this and other modeling approximations will be investigated and discussed further in Chapter 5.

3.4 The Proposed Distributed SWS Framework

A general framework of the distributed health monitoring technique implemented in this study is now outlined, cf. Figure 3.5.

Step I: SWSs are deployed onto the structure and a finite element model is developed. The mesh and sensor locations do not need to correspond exactly.

Step II: SWSs are initialized to gather “healthy” structural response data and to extract “healthy” observed features, $\{O_j\}$. The finite element model is used to simulate damage scenarios and to generate hypothetical damage features, $\{H_j\}$.

Step III: Hypothetical damage feature databases are wirelessly mapped (uploaded) to each deployed SWS. SWSs receive a particular damage identification database according to its spatial orientation on the structure.

In Figure 3.6 damage parameter, $X_j = 1 - DLAC_j$, graphically illustrates how the proposed distributed system would “show” damage during operation. The bar plots indicate the health of the structure spatially. It is important to note that each SWS would only need to transmit one number, X_j , drastically reducing the transmission load on the SWS.

⁴Per this author’s experience in industry, full-scale modal tests on civil infrastructure is too costly thus it not performed often. As such, some have looked at using ambient vibration records to update models of civil structures.

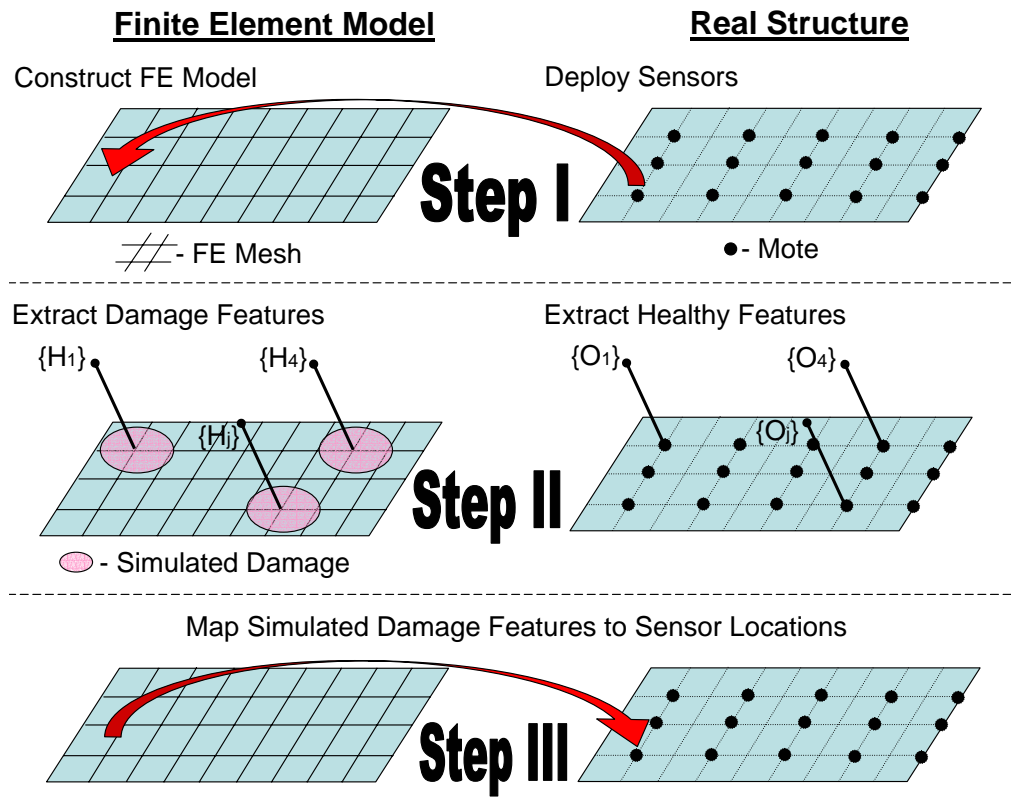


Figure 3.5: DLAC Smart Wireless Sensor Network Framework

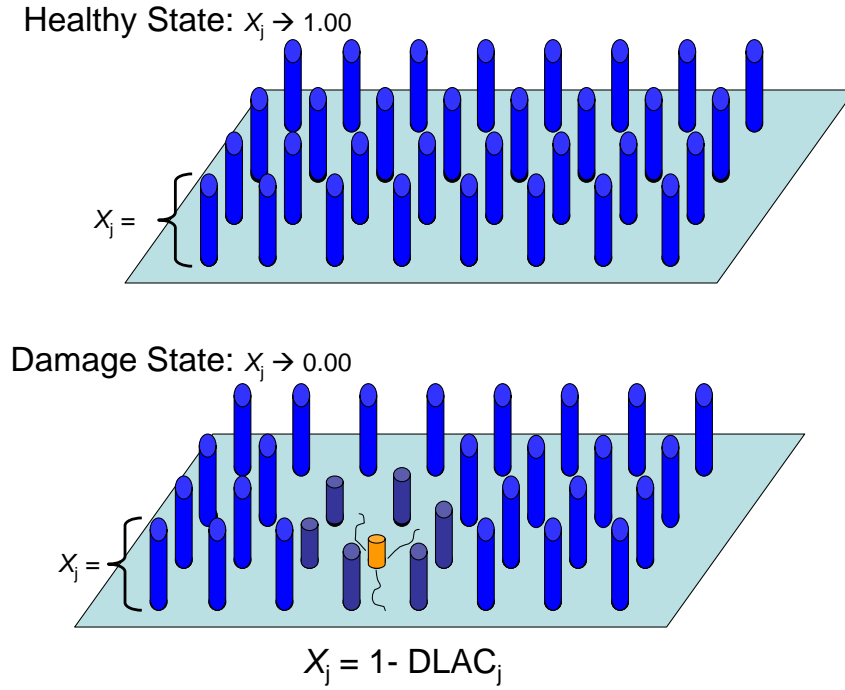


Figure 3.6: DLAC Smart Wireless Sensor Network Operation

3.5 Summary

In this chapter the motivation for developing a distributed SHM algorithm has been explained. The concept of health monitoring with a smart wireless sensor network versus that of monitoring with smart wireless sensors has been graphically illustrated. The principle behind feature correlation-based SHM paradigms has been introduced. Based on current power and data reliability limitations of commercially manufactured SWS, a natural frequency-based correlation technique known as the Damage Location Assurance Criterion (DLAC) was introduced for the studies conducted in this work. The DLAC metric and localization methodology can be implemented without multiple channels of synchronized data, thus is viable monitoring alternative for distributed structural health monitoring. Finally, the framework for using the proposed damage localization technique when implemented in a real structure was also presented. As such, in the forthcoming chapter the methodology will be validated experimentally.

Chapter 4

Algorithm and System Integration: Offline

4.1 Overview

In this chapter the DLAC correlation-based health monitoring approach is verified for smart wireless sensor network (SWSN) implementation. Two damage localization studies were conducted in the laboratory environment, one with a slender cantilever beam (a continuous system) and the other with a five storey shear building model (a lumped parameter system).

When these experiments were conducted in the spring and summer of 2005 commercially manufactured state-of-the-art motes did not yet encompass computational processors or data storage facilities suitable for embedded feature extraction algorithms. Recall, feature identification (extraction) is requisite for the DLAC method. At that time these limitations were attributed to the infancy of mote technology itself. In general, hardware developers did not know what performance specifications would be required for embedded feature extraction and health monitoring algorithms. There is also a cost-benefit analysis driving the product development. In this case the tradeoffs between increased computational horsepower, component cost and energy consumption were surely considered during the development.

The experiments presented in this chapter utilize raw data, wirelessly streamed from each mote to a central data collection station. Feature extraction and DLAC metrics were post-processed, but the offline calculations were conducted in a fashion consistent

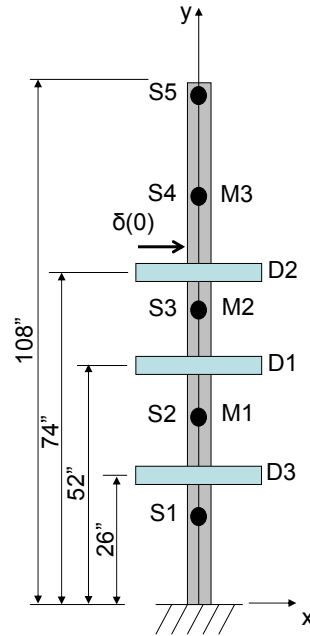


Figure 4.1: Cantilever Beam Setup (not to scale)

with that of a distributed sensor network. The goal of these preliminary investigations is to study the feasibility of implementing a SWSN consisting of unmodified off-the-shelf motes for Level II SHM.

4.2 A Slender Cantilever Beam

Here the efficacy of the DLAC monitoring methodology with Crossbow Technology's Mica2 motes was verified with a damage detection and localization experiment. The laboratory test structure was a 108 x 3 x .25 inch slender steel cantilever beam, cf. Figure 4.1.

Damage is simulated in this study by clamping a bar mass equivalent to 10 percent of the total beam mass onto the structure. Three single damage configurations were tested in this study and are denoted as D1, D2, and D3 in Figure 4.1. D1, D2, and D3 are approximately 52, 74, and 26 inches from the base of the beam, respectively.

Localizing damage at each of the three selected damage sites is considered to be of varying levels of difficulty. The effect of the lumped mass on the modal parameters becomes more pronounced as the mass moves further from the fixed boundary condition. As such, the effect of the mass on the characteristics will lessen as it tends toward the fixed end of the beam, making localization via frequency changes more challenging. This was done to test the robustness of the DLAC technique and the sensitivity of the sensor hardware.

Excitation was provided by striking the beam. The beam was struck at a location where the first four modes of vibration were those primarily excited. The strike location was consistent throughout all tests and its relative location on the beam has been denoted by the Dirac delta in Figure 4.1.

The structure was instrumented with three motes at locations M1, M2, and M3, cf. Figure 4.1. For response comparison five wired accelerometers were also installed at equally spaced intervals along the length of the beam, denoted as S1, S2, S3, S4, and S5 in Figure 4.1.

As previously discussed, the DLAC metric requires a numerical model of the structure to generate natural frequencies for each simulated damage case. In this study, Euler-Bernoulli finite element beam models of various refinements, i.e. number of elements, were created to evaluate the performance of the method. It is important to note that while there is little variation in the first four natural frequencies of a numerical model consisting of five or more elements, the refinement of the beam model affects the performance of the DLAC localization metric. As such, a few models of various refinements were implemented to highlight this point. A thorough sensitivity analysis of the DLAC method is presented in Chapter 5.

In Table 4.1 the first four analytical natural frequencies for each configuration are presented. A 50 element numerical model of the beam was created to approximate the actual structure's modal frequencies. In all numerical models used in this study the following nominal properties were taken to simulate steel: Young's Modulus of 30,000 ksi and density of 15.23 lbm/ft³.

Table 4.1: Natural Frequencies (Hz): FE Model

Mode	ω_{Hlth}	ω_{D1}	ω_{D2}	ω_{D3}
1	0.70	0.69	0.66	0.70
2	4.39	4.02	4.28	4.26
3	12.28	12.24	11.49	11.27
4	24.06	22.43	23.77	22.38

4.2.1 Hardware

The MPR410CB Mica2 motes were connected to MTS310CA multi-sensor boards to acquire acceleration measurements. The Mica2 mote is a tiny embedded computing platform roughly the size of a matchbox and operates on two AA batteries. The performance specifications of the device are listed in Table 4.2

Table 4.2: Performance Specifications: Mica Series Motes [11]

<i>Feature</i>	Mica2	MicaZ
<i>A/D Channels</i>	8	8
<i>Sample Rate</i>	1 kHz [33]	1 kHz [33]
<i>A/D Resolution</i>	10-bit	10-bit
<i>Processor</i>	Atmel ATmega128L	Atmel ATmega128L
<i>Bus Size</i>	8-bit	8-bit
<i>Clock Speed</i>	7.37 MHz	7.37 MHz
<i>Program Memory</i>	128 kB	128 kB
<i>Data Memory</i>	512 kB	512 kB
<i>Radio</i>	Chipcon CC1000	Chipcon CC2420
<i>Frequency Band</i>	315/433/915 MHz	2400 MHz
<i>Data Rate</i>	38.4 kbps	250 kbps
<i>Max Tx Range</i>	1000 ft	328 ft
<i>Dimensions</i>	1.25 x 2.25 x 0.25 in	1.25 x 2.25 x 0.25 in
<i>Max Current Draw</i>	25 mA	19.7 mA
<i>Power Source</i>	Battery (3V)	Battery (3V)

It is important to note that the performance specifications on the CC1000 radio are theoretical limits. As its 38.4 kbps bandwidth and 1000 ft communication range vary substantially over time and space [61]. Taking into consideration these limitations

10 data points are acquired, temporarily cached, then sent as a single package to the base station thereby reducing the wireless transmission load.

The base station is connected to a laptop via a serial link, and in this experiment it simply forwards all messages to the laptop. The laptop runs a Java application that logs the data for subsequent offline post-processing analysis. Each group of 10 measurements within a message package is tagged with a sequence number and source mote ID number, allowing the data logger to correctly arrange the resulting data.

The Mica2 mote use a simple carrier sense multiple access contention avoidance (CSMA-CA) protocol for taking ownership of the radio channel [55]. A CSMA networking procedure is simple implement, however it does not have deterministic transmission characteristics [57]. Since full ownership of a radio channel is allowed, bandwidth contention is a problem when several motes are required to transmit data simultaneously as in this study. The result of this is message loss due to wireless data collisions. Recall, each message contains ten measurements, thus one lost message will result in the loss of ten sensor readings. Complex acknowledgement and retransmit schemes were not implemented in this study to avoid problems due to additional overhead and worsened radio contention.

Under a CSMA networking procedure message loss will increase as the number of motes transmitting data is increased and/or the sampling frequency is increased. Mica2 motes have a software programmable analog-to-digital converter onboard so the frequency at which sensor is queried, i.e. the sampling frequency, can be adjusted. A parameter study was performed to determine the optimal sampling frequency for a multi-mote sensing configuration at sampling frequencies of 25 Hz, 100 Hz, and 200 Hz utilizing 2-4 motes simultaneously.

Despite better performance at lower sampling rates, the MTS310CA multi-sensor board is equipped with an accelerometer configured to a 50 Hz bandwidth. Sampling data at less than the Nyquist sampling frequency, in this case 100 Hz, will result in aliased data which can greatly reduce the performance of the localization procedure. Data acquired at sampling rates of 200 Hz suffered transmission datalosses of more than 50 percent at times and was deemed too unreliable for use in the study.

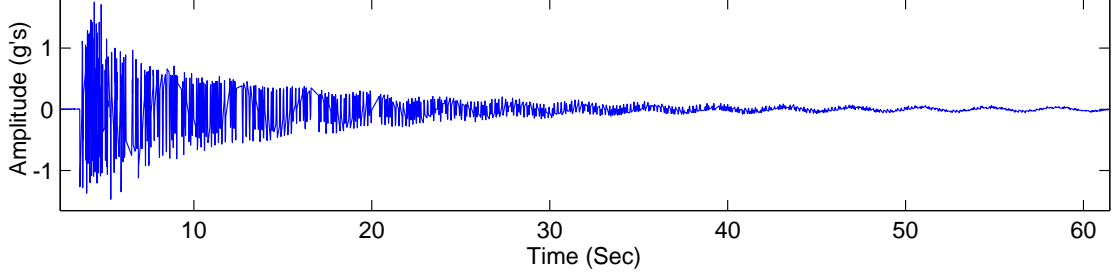


Figure 4.2: Transmission Data Loss in Time History, $F_s = 100$ Hz

Table 4.3: Performance Specifications: ADXL202JE MEMS Accelerometer [1, 11]

No. Channels	2
Range	± 2 G
Bandwidth*	50 Hz
Sensitivity	167 mV/G ± 17 %
Resolution	2 mG
RMS Offset	VBattery/2 ± 0.4 V

* As configured on MTS310CA.

All data acquired and presented in this study was obtained using three motes simultaneously, each sampling at a 100 Hz. Since unsynchronized data was acquired, fairly reliable transmissions could be made at 100 Hz. The response time history shown in Figure 4.2 illustrates the nominal¹ amount of data loss observed during experiments utilizing three motes at 100 Hz sampling frequency.

The ADXL202JE is a dual-axis MEMS accelerometer developed and manufactured commercially by Analog Devices. This device operates with an extremely low current draw <1 mA and produces a duty cycle modulated digital output in addition to a standard analog output. If configured correctly the ADXL202 is quite suitable for smart wireless sensor applications² [1, 11]. A list of the ADXL202JE's performance specifications have been listed in Table 4.3.

¹Since CSMA protocol does not have deterministic transmission characteristics test results varied.

²Refer to Appendix B for more information about configuring the ADXL202JE.

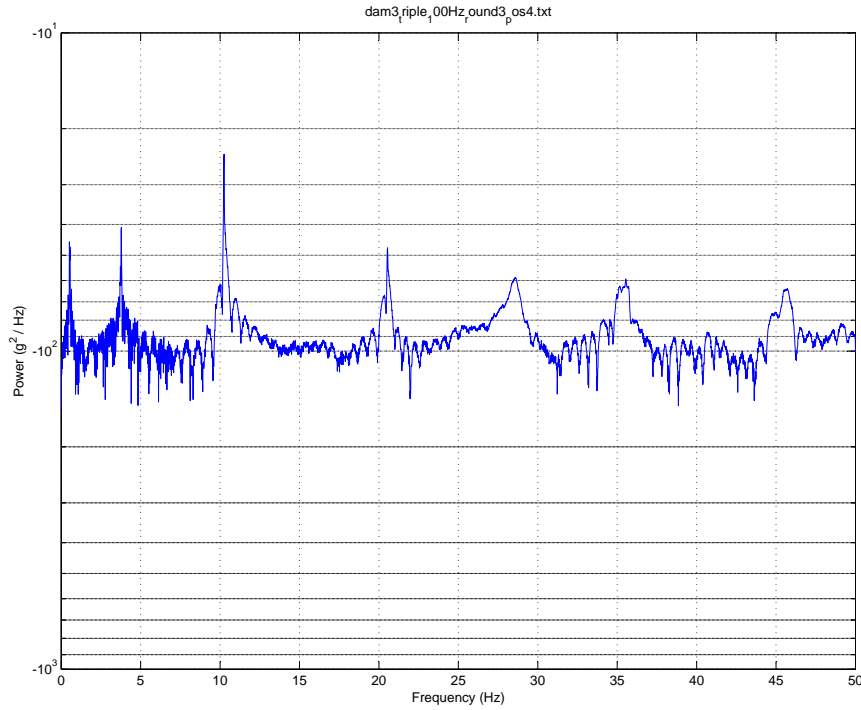


Figure 4.3: Power Spectrum of System with Damage at Location D3

4.2.2 Frequency Identification

Raw time history data was received at the base station and stored on a portable computer before being processed. Spectral analysis of the response time histories was completed using MATLAB via the periodogram method. To construct a response power spectrum a boxcar window was applied to a 1024 point buffered frame of time history. As such no averaging in the time domain occurred. Natural frequencies of the cantilever beam were identified by manually selecting the peaks in the power spectrum. A typical power spectrum is shown as Figure 4.3. Frequencies identified over various test runs were subsequently averaged.

To determine each set of “healthy” and “damaged” natural frequencies, eight impulse tests were conducted and the identified frequencies were averaged. As configured on the MTS310CA sensor board the resolution of the ADXL202JE accelerometer was compromised at higher frequencies. Even though seven natural frequencies of the beam were within the sensor bandwidth, only the first four natural frequencies could be identified accurately. This resolution problem can be observed in Figure 4.3.

Table 4.4: Natural Frequencies Identified (Hz): Mica2 Motes

Mode	ω_{Hlth}	ω_{D1}	ω_{D2}	ω_{D3}
1	0.54	0.51	0.48	0.53
2	3.91	3.61	3.83	3.82
3	11.16	11.16	10.46	10.25
4	21.95	20.49	21.46	20.54

Table 4.5: Natural Frequencies Identified (Hz): Wired System

Mode	ω_{Hlth}	ω_{D1}	ω_{D2}	ω_{D3}
1	0.50	0.50	0.50	0.50
2	4.00	3.75	4.00	3.88
3	11.50	11.50	10.75	10.50
4	22.63	21.00	22.13	21.25

Notice the three distinct peaks above 25 Hz are rounded apposed to the four distinct sharp peaks below 25 Hz.

Natural frequencies experimentally identified with Mica2 mote technology are presented in Table 4.4. Frequencies identified with traditional wired instrumentation are in fair agreement with those obtained with motes, cf. Table 4.5.

Variations in the results presented in Table 4.4 and Table 4.5 may be attributed in part to a small variation in the structure's mass during testing since the battery powered motes were not attached while data was acquired for wired test. This explanation is consistent with the slightly higher frequencies observed in modes 2-4 of Table 4.5.

Despite the discrepancies noted between the wired and wireless frequencies a distinct shift between healthy and damaged frequencies is still apparent, thus damage can be detected. Significant deviations in natural frequencies exist between those obtained experimentally and byway of the FE model. These differences are most likely attributed to an imperfect clamped boundary condition and a geometric stiffness loss attributed to the vertical configuration of the slender beam. Both contributions were neglected in the numerical model of the structure. In practice, a high-fidelity, tuned FE model of an as-built civil engineering structure is often unavailable. Thus, damage detection methodologies should be robust to modeling errors such as the type possibly

observed here. Therefore in an effort to evaluate the robustness of the technique to actual implementation conditions the FE model was not updated in this study.

4.2.3 Damage Localization

In this study three different numerical “identification” models were developed to simulate structural damage. Each model was used to generate a database of hypothesis frequency change vectors which will be correlated to the experimental change vectors using DLAC method, cf. Equation 3.1. Recall, that a correlation factor equal to unity represents perfect co-linearity of the hypothesis and experimental frequency change vectors. Since experimental error exists, damage is said to be localized to areas where the DLAC value tends to unity.

The performance of the DLAC method was tested with different three identifications models using various numbers of natural frequencies.

Initially, a 50 element numerical model is used to identify damage. The model simulated a particular damage case by lumping a mass equivalent to 20 percent of the total beam mass at one node. Thus a database suite of 51 hypothesis frequency change vectors was created. Figure 4.4 clearly depicts the location of the bar mass on the beam for each experiment and the variation of the DLAC metric along the length of the beam. Here all four of the experimentally identified natural frequencies were used in the correlation. (equivalent to a 10 percent increase in mass) It is obvious that peak DLAC metrics accurately indicate the correct location of damage in all three cases.

Figure 4.5 and Figure 4.6 demonstrate the performance of the DLAC method with respect to modal truncation (no. of modes) and spatial quantization (no. of elements) of the frequency database. Both models generate hypothesis frequency change vectors using a lumped mass which simulates various percentages of the total beam mass.

For this simple structure it is interesting and advantageous to note that damage can be localized in some cases with as few as two modal frequencies. Also, notice that little is gained by increasing the identification model from 20 elements to 216

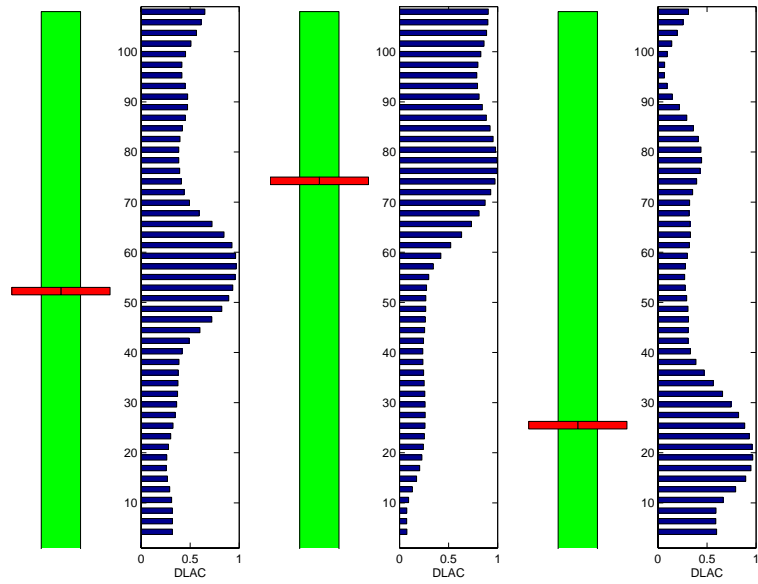


Figure 4.4: DLAC Localization: 51 Node Model, 20% Simulated Damage, 4 Modes

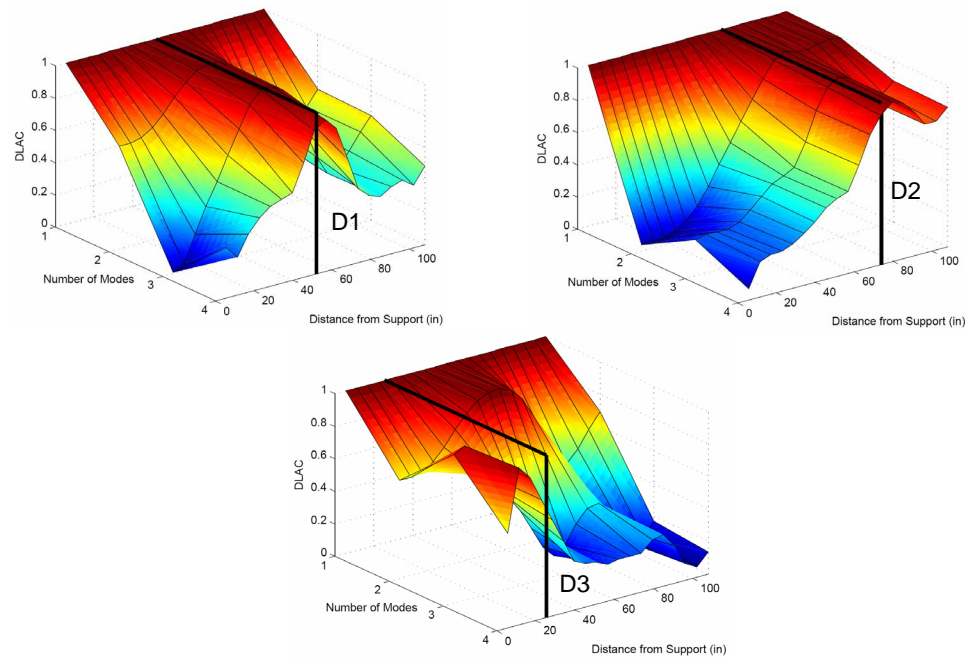


Figure 4.5: DLAC Localization: 19 Node Model, 500% Simulated Damage

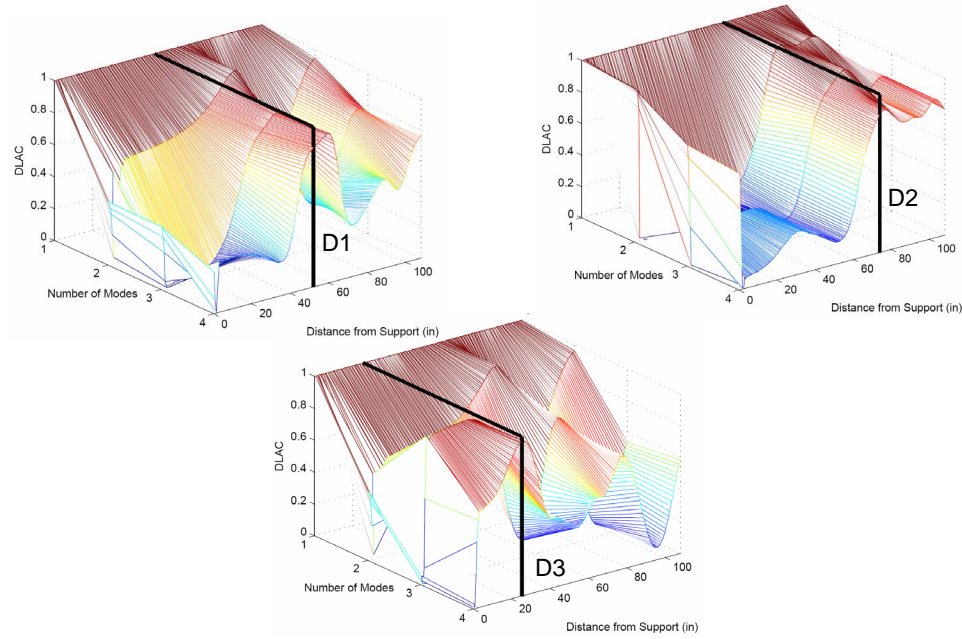


Figure 4.6: DLAC Localization: 215 Node Model, 10% Simulated Damage

elements. The 216 element model also simulates the same magnitude of damage as that actually imposed on the beam during the experiments, whereas the damage simulated with the 20 element model is much more than that truly imposed.

These observations make feature correlation-based health monitoring even more attractive for distributed smart wireless sensor networks. It is often difficult to experimentally acquire large numbers of modal frequencies especially with the present sensor hardware. Moreover, large identification models are computationally intensive to develop and require large memory banks to store the frequency database.

The results of a more comprehensive investigation of spatial quantization and modal truncation are presented in Chapter 5 of this work.

4.3 Five Storey Shear Building Model

Here the efficacy of the DLAC monitoring methodology with Crossbow Technology's MicaZ motes was verified with a damage detection and localization experiment. In

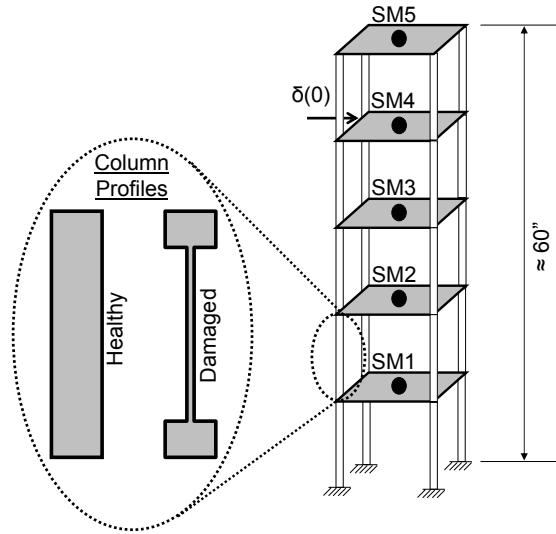


Figure 4.7: Building Model Setup (not to scale)

this study a five bay lumped mass shear building model was selected as the test structure, cf. Figure 4.7.

Damage was induced to the structure by reducing the inter-storey column stiffness. This stiffness reduction was facilitated by exchanging the original columns by those with a lesser moment of inertia. By replacing two of the four “healthy” inter-storey columns with “damaged” column profiles the cumulative inter-storey stiffness was reduced by 33 percent, cf. Figure 4.7. Only single storey damage scenarios were investigated in this study.

To excite the structure for testing an impulse load was generated along the global x-axis by striking the 4th floor of the structure with a modally tuned impact hammer. Acceleration response time histories were simultaneously recorded with both MicaZ motes and wired AC accelerometers. These devices were installed on each floor of the model and were co-located at SM1–SM5, cf. Figure 4.7. The sensing equipment was configured to acquire accelerations only in the direction of input excitation.

A coarse five Euler-Bernoulli element numerical model of the shear building was created to postulate the actual structure’s modal frequencies. In Table 4.6 five analytical natural frequencies of each damage configuration are presented. Each steel floor diaphragm was modeled as a lumped mass of 0.167 slugs. Each healthy column had a

Table 4.6: Natural Frequencies (Hz): FE Model

Mode	ω_{Hlth}	ω_{FD1}	ω_{FD2}	ω_{FD3}	ω_{FD4}	ω_{FD5}
1	3.34	3.00	3.04	3.12	3.22	3.30
2	9.72	8.98	9.64	9.38	8.76	9.01
3	15.38	14.73	14.75	14.18	15.26	13.85
4	19.66	19.28	18.01	19.47	18.48	18.69
5	22.56	22.46	22.01	21.17	21.56	22.26

width of 1.18 inches, a thickness of 0.10 inches, and an effective length of 9.45 inches. Damaged columns had the same dimensions except the width was modified to 0.24 inches. All columns were bronze as such a nominal Young’s Modulus of 14,500 ksi was used. Additional mass attributed to the columns was neglected.

4.3.1 Hardware

In this study Crossbow Technology’s MPR2400CB MicaZ motes were connected to MTS310CA multi-sensor boards to acquire acceleration measurements. The MicaZ mote is identical to the Mica2 mote except for its Chipcon CC2420 radio transmitter, cf. Table 4.2. The CC2420 radio operates in the unlicensed 2.4 to 2.4835 GHz band and is compatible with the IEEE 802.15.4 Zigbee standard. It is more power efficient than the Mica2’s CC1000 radio and offers a maximum theoretical bandwidth of 250 kbps, more than six times that of the Mica2 bandwidth. The only potential drawback of the MicaZ mote’s CC2420 radio is that its transmission range is reduced to a theoretical maximum of approximately 328 feet.

As with the Mica2 mote, structural response time histories were acquired the MTS310CA multi-sensor board. Recall this board implements the ADXL202JE MEMS accelerometer, cf. Table 4.3. Response time histories acquired were not processed or stored onboard. Instead synchronized time histories of response data were streamed directly from all four motes simultaneously to a base station and stored on a PC.

In this study wireless data acquisition was synchronized and transmitted to a base station in real time. As such, data loss due to contention of the wireless link was presumed to be a serious issue as it was in a previous study with Mica2 motes.

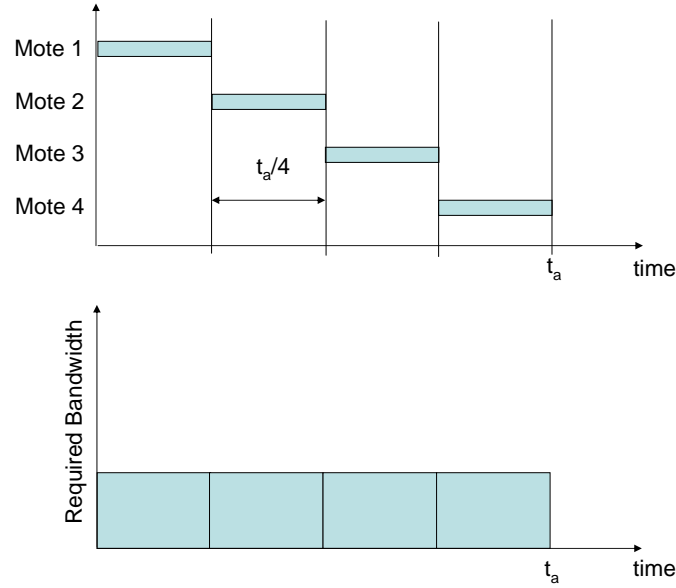


Figure 4.8: TDMA Transmission Schedule Example

To circumvent the potential problem of radio bandwidth contention a staggered transmission protocol similar to Time Division Multiple Access (TDMA) was implemented on top of the default Medium Access Control protocol (B-MAC) provided by the TinyOS operating system [47]. TDMA is a networking procedure currently used by GSM (Global System for Mobile) digital cellular systems in Europe and Asia [57]. Essentially it is a time-division multiplexing procedure for dividing a radio frequency into discrete time slots and then allocates the slots to multiple data streams. As a result, a single frequency band can support multiple channels of data which are streaming simultaneously [57].

An illustration of the TDMA like networking protocol implemented in this study is presented as Figure 4.8. Each mote is configured to package 10 data points in each transmission. Based on rate at which data is be sampled the total data acquisition time is calculated, t_a . Then the total data acquisition time is divided into an equal number of transmission time slots based number of motes acquiring data. For a four mote network simultaneously sampling data 100 Hz, 10 data points take 100 ms to acquire, so a 25 ms transmission window is assigned to each mote. The result of a specifying a unique transmission time slot increases the reliability of data transfer as motes do not contend for bandwidth.

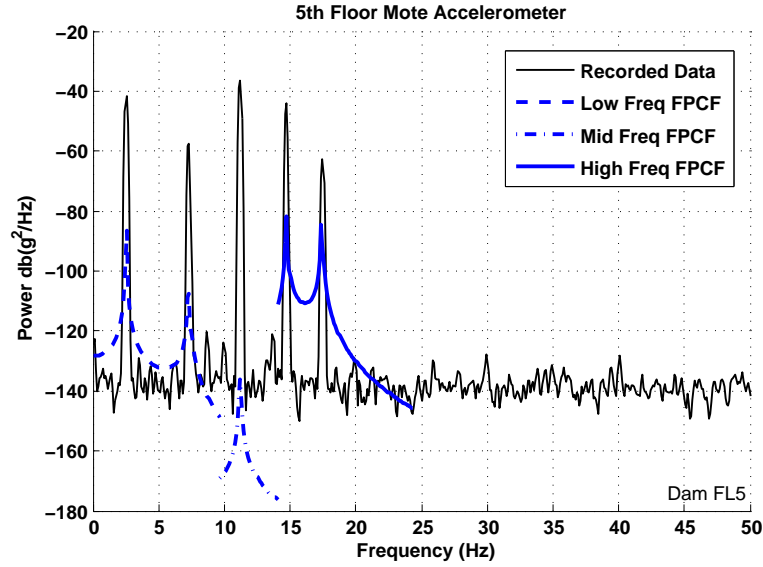


Figure 4.9: FPCF Wireless Sensor Data

4.3.2 Frequency Identification

The DLAC method functions by correlating observed natural frequency changes with those simulated to detect and localize damage. As such, the numerical model of the structure required for localization can also be used to develop or train an automated feature extraction program.

In accordance with the constraints of an embedded decentralized health monitoring system, Levy's automated frequency extraction technique, presented in Chapter 2, was tested [30]. An empirical study indicated that all of the modes of the experimental system tested in this study could be identified using the Fractional Polynomial Curve-fitting (FPCF) technique. To ensure reliable characterization of resonant frequencies, three fractional polynomials were defined over three piecewise discontinuous frequency bands. As such, fractional polynomials were fit to the test data over a low, mid, and high frequency band for each experiment. The three frequency bands were determined from the approximate modal frequencies obtained from the numerical identification model of the structure. Figure 4.9 illustrates graphically the accuracy of the FPCF technique discussed here.

Identified Resonant Frequencies Wired Accerometer Data						Identified Resonant Frequencies Wireless Accerometer Data					
HEALTHY	<i>mode I</i>	<i>mode II</i>	<i>mode III</i>	<i>mode IV</i>	<i>mode V</i>	HEALTHY	<i>mode I</i>	<i>mode II</i>	<i>mode III</i>	<i>mode IV</i>	<i>mode V</i>
Manual	2.64	7.72	12.30	15.82	18.26	Manual	2.54	7.52	12.01	15.53	17.77
ERA	2.59	7.71	12.33	15.86	18.21	ERA	2.52	7.51	12.02	15.46	17.75
FPCF	2.60	7.72	12.33	15.87	18.22	FPCF	2.52	7.53	12.03	15.48	17.77
Damg FL1	<i>mode I</i>	<i>mode II</i>	<i>mode III</i>	<i>mode IV</i>	<i>mode V</i>	Damg FL1	<i>mode I</i>	<i>mode II</i>	<i>mode III</i>	<i>mode IV</i>	<i>mode V</i>
Manual	2.34	7.23	11.91	15.62	18.16	Manual	2.34	7.03	11.72	15.33	17.68
ERA	2.37	7.23	11.95	15.66	18.17	ERA	2.30	7.04	11.65	15.27	17.72
FPCF	2.37	7.23	11.94	15.67	18.16	FPCF	2.31	7.05	11.66	15.29	17.73
Damg FL2	<i>mode I</i>	<i>mode II</i>	<i>mode III</i>	<i>mode IV</i>	<i>mode V</i>	Damg FL2	<i>mode I</i>	<i>mode II</i>	<i>mode III</i>	<i>mode IV</i>	<i>mode V</i>
Manual	2.44	7.72	11.91	14.84	17.97	Manual	2.34	7.52	11.62	14.45	17.48
ERA	2.41	7.74	11.89	14.85	17.92	ERA	2.35	7.55	11.60	14.49	17.49
FPCF	2.43	7.74	12.28	14.85	17.94	FPCF	2.35	7.55	11.60	14.49	17.49
Damg FL3	<i>mode I</i>	<i>mode II</i>	<i>mode III</i>	<i>mode IV</i>	<i>mode V</i>	Damg FL3	<i>mode I</i>	<i>mode II</i>	<i>mode III</i>	<i>mode IV</i>	<i>mode V</i>
Manual	2.44	7.52	11.72	15.62	17.48	Manual	2.44	7.32	11.43	15.23	16.99
ERA	2.48	7.50	11.70	15.63	17.45	ERA	2.41	7.30	11.40	15.22	17.02
FPCF	2.49	7.52	11.71	15.65	17.48	FPCF	2.44	7.30	11.43	15.59	17.02
Damg FL4	<i>mode I</i>	<i>mode II</i>	<i>mode III</i>	<i>mode IV</i>	<i>mode V</i>	Damg FL4	<i>mode I</i>	<i>mode II</i>	<i>mode III</i>	<i>mode IV</i>	<i>mode V</i>
Manual	2.54	7.13	12.21	15.53	17.38	Manual	2.44	6.93	11.91	15.14	16.99
ERA	2.54	7.12	12.18	15.47	17.38	ERA	2.45	6.91	11.85	15.05	16.90
FPCF	2.55	7.13	12.20	15.49	17.38	FPCF	2.48	6.95	11.89	15.10	16.96
Damg FL5	<i>mode I</i>	<i>mode II</i>	<i>mode III</i>	<i>mode IV</i>	<i>mode V</i>	Damg FL5	<i>mode I</i>	<i>mode II</i>	<i>mode III</i>	<i>mode IV</i>	<i>mode V</i>
Manual	2.64	7.52	11.52	15.14	17.97	Manual	2.54	7.32	11.23	14.75	17.48
ERA	2.60	7.46	11.48	15.09	17.91	ERA	2.51	7.25	11.17	14.67	17.42
FPCF	2.62	7.48	11.50	15.12	17.91	FPCF	2.53	7.28	11.20	14.72	17.41

Figure 4.10: Experimentally Identified Resonant Frequencies

It should also be noted that the piecewise FPCF scheme presented here performed robustly to frequency shifts incurred by damages. Therefore the “healthy” frequency band limits specified for each fractional polynomial $H(i\omega)$, recall Equation 2.19, remained the same for all tested damage scenarios.

Wired and wireless acceleration impulse response time histories were acquired simultaneously during experimentation. Time histories were then post-processed on a PC to identify the resonant frequencies of the test structure. A direct comparison between frequencies identified by manual spectrum peak picking, the Eigensystem Realization Algorithm (ERA) and Fractional Polynomial Curve-fitting (FPCF) is shown with good agreement in Figure 4.10.

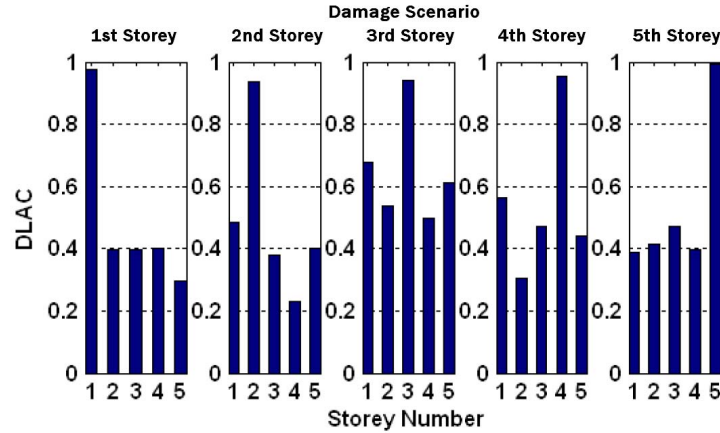


Figure 4.11: DLAC Localization Result

4.3.3 Damage Localization

A simple 5 degree-of-freedom lumped parameter numerical beam model was used as the identification model in this study. Each damage scenario was simulated with a 10 percent reduction in inter-storey column stiffness. The results of the DLAC correlation are presented in Figure 4.11.

4.4 Summary

In this chapter damage identification and localization has been successfully performed with both the Mica2 and MicaZ mote sensors. The MTS310 multi-sensor board proved to capture accurate response behavior below 25 Hz and despite data losses attributed to wireless transmissions the natural frequencies obtained corresponded well with those identified using wired accelerometers and more sophisticated signal processing software.

Both the sensors and the DLAC correlation procedure proved to perform robustly when applied to either a continuous or lumped parameter system. An advantage of this approach was shown in its capacity of localizing damage with data collected by wireless sensors and “first round” numerical models, i.e. those which have not been dynamically tuned or updated.

The DLAC health monitoring technique has been developed for implementation as part of distributed smart wireless sensor network. The next step is to embed the DLAC algorithm on a smart wireless sensor.

Chapter 5

DLAC Sensitivity Analysis

5.1 Motivation

The Damage Location Assurance Criteria (DLAC) and localization methodology were developed in 1996 by Messina, Jones, and Williams [38]. In their developmental paper a significant portion of this work was focused on assessing the reliability of the DLAC metric. As such, a series of numerical simulations were conducted to evaluate its performance with respect to various levels of noise and modal truncation. While the paper presented results which illustrate the DLAC method is more effective than Crawley and Adams' (1979) localization algorithm, the study itself is not well suited for evaluating the practical efficacy of the DLAC metric or localization procedure [5]. It appears that the nature of the investigation, i.e. a completely nonphysical one (numerical simulation), allowed Messina, Jones, and Williams to make a few oversights regarding the effects of the following items,

- the resolution of the identification model versus the refinement of the “actual” model (*Spatial Quantization*).
- the effects of the distribution of noise used to generate “actual” modal frequencies (*Simulation Noise Distribution*).
- the validity of a reliability analysis based on absolute correlation (*Absolute DLAC Correlation*).

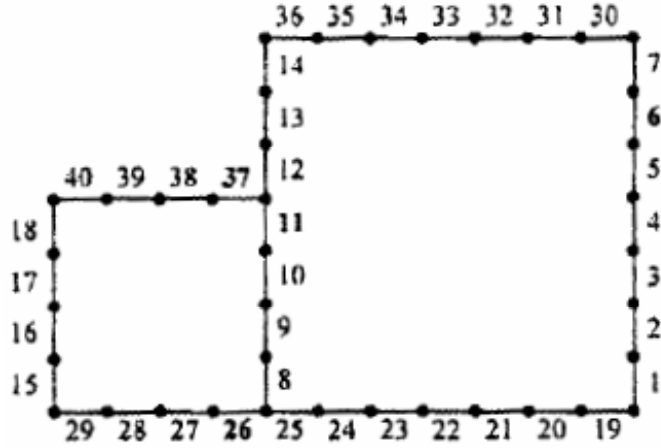


Figure 5.1: Messina *et al.* (1996) DLAC Validation Model [38]

5.1.1 Spatial Quantization

Consider the numerical validation model used by Messina *et al.*, cf. Figure 5.1. This validation model was used as both the “actual” structure and the identification model for the localization procedure in the study. In practice it is far too computationally intensive to develop extremely refined finite element models of large civil structures. (Such an occurrence might be plausible for stress analysis, however often only portions of the structure are modeled for this purpose.) Even if such a large numerical model was developed, it is not likely that its dynamic behavior would match that of the actual structure’s beyond the first or second mode. A complete modal survey of the actual structure would need to be conducted in order to update, or tune, the identification model’s modal characteristics. Moreover, creating the required database of modal characteristics for each damage scenario simulated would again prove to be too computationally intensive. As such, to be practical it makes sense to evaluate the effectiveness of the DLAC localization technique using a coarse, or reduced, damage identification model. This introduces a loss of resolution in the DLAC localization procedure, which will be called *spatial quantization* in this study.

Spatial quantization as it is conceptualized here is the condensation of the actual structure’s infinite degrees of freedom to that of the identification model’s finite degrees of freedom. The intrinsic result of spatial quantization is a direct reduction in the resolution of the damage detection algorithm.

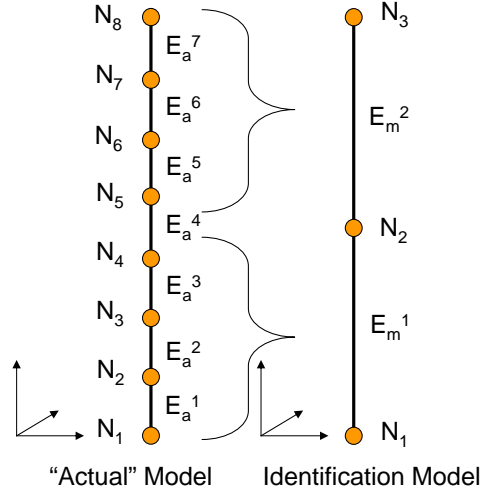


Figure 5.2: Spatial Quantization

For example, consider the illustration shown in Figure 5.2. Notice the actual structure is prescribed to have 7 elements and the identification model, used to generate all of potential damage scenarios, has only 2 elements. Even though the real structure could be damaged in any of the 7 element using the 2 element identification model there are only two possible outcomes. As such, the DLAC spatial resolution has been quantized to:

1. $\{E_a^1, E_a^2, E_a^3\} \in E_m^1$
2. $\{E_a^5, E_a^6, E_a^7\} \in E_m^2$

5.1.2 Simulation Noise Distribution

It makes sense to attempt to simulate uncertainties associated the real-world, i.e. in-situ operation of frequency extraction algorithms, by adding noise to analytical measurements. Consider the arguments graphically presented in Figure 5.3. As discussed in Chapter 4, automated frequency extraction can often be completed by fitting a fractional polynomial (FPCF) to an experimental power spectral density (PSD) of the structure's response behavior. As with any curve-fitting technique there are usually slight errors associated with the natural frequencies extracted via FPCF

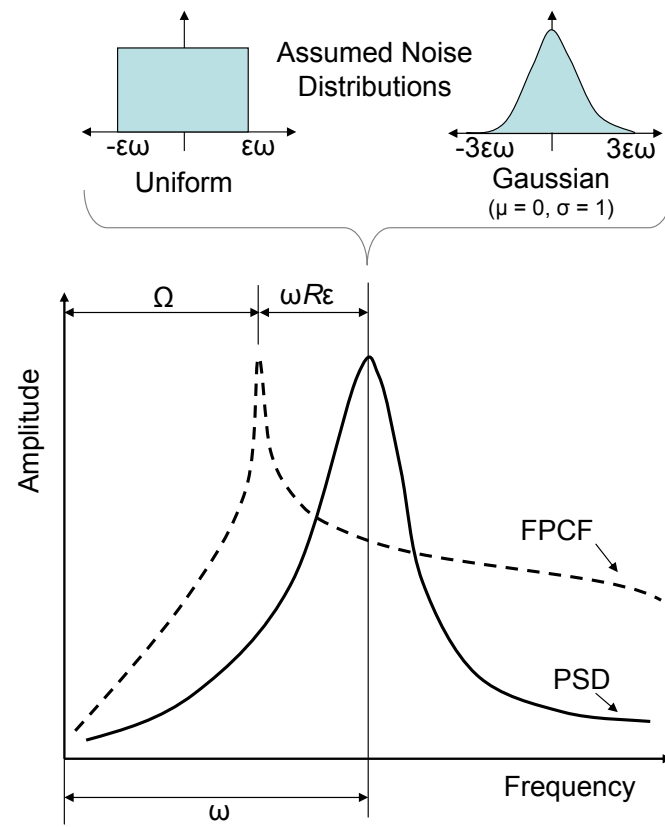


Figure 5.3: Errors Attributed to Automated Frequency Extraction

and those of the actual structure, cf. Figure 5.3 (exaggerated). As such, when completing a numerical simulation this uncertainty can be introduced when generating the “actual” structure’s natural frequencies. Typically this is done by seeding the natural frequencies of the identification model with noise. Therefore, for any particular natural frequency of the identification model, ω , a corresponding “actual” natural frequency of the structure, Ω , may be simulated according to the following expression

$$\Omega = \omega + \omega R\epsilon \quad (5.1)$$

where, R is a randomly distributed number and ϵ is the percentage of imposed measurement error, as illustrated in Figure 5.3. Notice that in Equation 5.1, the imposed measurement error, scaled by ω and ϵ , is added to natural frequencies, ω . In Messina, Jones, and Williams’ study it is uncertain if “actual” natural frequencies were generated in the same fashion.

In Messina *et al.*’s study an expression which seeds noise to natural frequency changes, $\delta\omega$, appears to have been implemented [38], cf. Equation 5.2.

$$\delta\Omega = \delta\omega + \omega R_u\epsilon \quad (5.2)$$

Notice that experimental natural frequency changes, $\delta\Omega$, are developed from noise scaled by, ϵ , R_u , and natural frequencies themselves, ω , not by natural frequency changes. This formulation of noise is acceptable if absolute frequency changes are used, as shown in Equation 5.3.

$$\delta\omega = \omega_{\text{health}} - \omega_{\text{observed}} \quad (5.3)$$

However, one of the studies conducted was based on the a fractional frequency change, cf. Equation 5.4.

$$\delta\omega = \frac{\omega_{\text{health}} - \omega_{\text{observed}}}{\omega_{\text{health}}} \quad (5.4)$$

If Equation 5.2 was used for this portion of the analysis the generated frequency changes, $\delta\Omega$, would be flawed. This can be shown by dimensional analysis, i.e. realizing the units for each term of Equation 5.2 are inconsistent. No commentary was provided by the authors to assure the reader this minor, yet influential, detail was

not overlooked during the fractional frequency feature analysis. Moreover, the authors generated noise with a uniformly distributed random number, R_u , which has a range of -1 to +1 without offering any explanation as to why this type of distribution was selected, cf. Equation 5.2 [38]. It seems reasonable to tie this back the physical behavior of the system and if the behavior is unknown, perhaps a suite of various distributions should be used.

5.1.3 Absolute DLAC Correlation

The reliability of the DLAC localization procedure, as defined by Messina *et al.*, is determined by a DLAC of unity, indicating perfect correlation [38]. As such, success rates were calculated in the following manner. If for a given simulation iteration the $DLAC = 1$, then this trial is deemed a success. Thus, the success rate of a simulation is the total number of successes divided by the number times the test was iterated. Within the confines of the nonphysical realm of the computer this type of absolute success rate analysis is appropriate and justified. Although in practice, perfect unity correlation coefficients are rarely observed, cf. Figure 4.4 and Figure 4.11. More often than not the DLAC analysis yields results which can only provide indications as to where structural damage may be, i.e. $DLAC \rightarrow 1$. The sensitivity analysis performed in Messina's study is a conservative first approximation, however in this study a metric is developed which takes into consideration the realistic behavior of DLAC correlation coefficient tendencies as observed in practice.

Based on the motives presented herein the reliability of the DLAC method will be reassessed to address the issues of spatial quantization, simulation noise distribution, and non-absolute correlation coefficients. To make these improvements the three following items will be implemented in the numerical study assessing the reliability of the DLAC localization method:

- identification and “actual” models of various *different* refinements ratios will be implemented.
- both uniform and Gaussian noise distributions will be implemented using Equation 5.1 to generate “actual” natural frequencies.

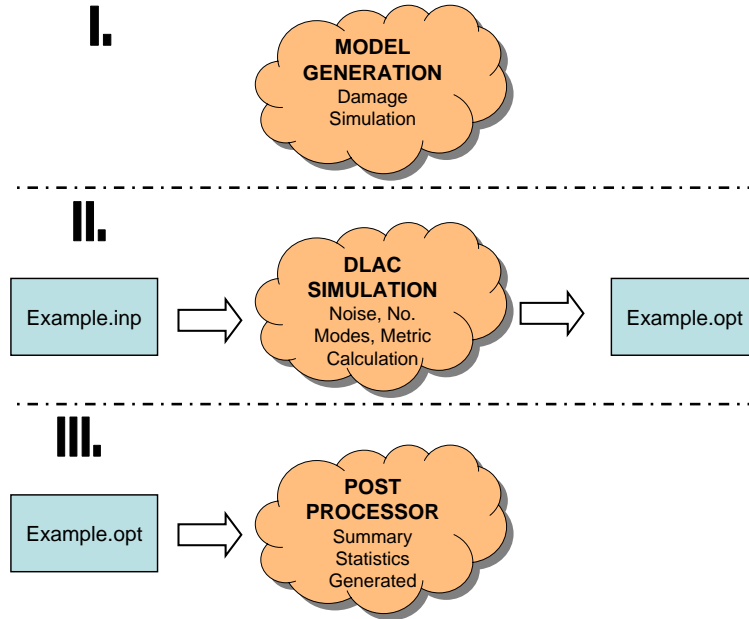


Figure 5.4: Process Diagram: Modeling and Simulation Procedure

- a correlation performance metric will be defined and success will be qualitatively assessed using this tool.

The cantilever beam structure used in the first offline localization experiment (Chapter 4) is used as the “test structure” for the numerical sensitivity analysis presented here, cf. Figure 4.1.

5.2 Simulation Procedure

To facilitate the intensive computational analysis presented in this chapter a three stage analysis program was created in MATLAB. The scheme of this program is outlined in Figure 5.4 and can be summarized into the following three levels.

Level I Here Euler-Bernoulli finite element beam models of various refinements are assembled and suites of natural frequencies are generated. There is one suite of frequencies per model generated. Suites consists of a set of natural frequencies

for each simulated damage location. In this study natural frequencies are perturbed to simulate damage and frequency perturbation is achieved by adding a lumped mass to individual nodes. For example, a 127 element (128 node) model would have 128 unique single damage scenarios, thus 128 sets of natural frequencies would be generated to comprise the suite.

Level II Here a user defined text file is accessed by the program. This input file consists of a list of FE models (created in Level I) which will be loaded into the DLAC simulation program for comparison. Within the input file the user also defines one particular FE model to be the simulated “actual” structure, all other FE models called in the input file are then used as identification models in the DLAC identification algorithm. Once the DLAC simulation program commences the user can select the number of modal frequencies for the correlation procedure and the percentage of measurement noise to impart on the system. All performance metrics are calculated here and then printed in an output file.

Level III Here several post-processing routines were created to generate the various success rate summary statistics from the information printed in the Level II output files. In this chapter the parameters which are investigated to determine their affect on the accuracy and overall efficacy of the DLAC method are spatial quantization, hypothesis damage intensity, and modal truncation with respect to noise.

5.3 Generalized Parameters

In an attempt to generalize the results presented in this chapter a few expressions are defined with respect to parameters of the “actual” model and the identification model.

Consider the model refinement metric, M , defined as,

$$M = \frac{NNIM}{NNAM} \quad (5.5)$$

where, NNIM is the number of nodes in the identification model and NNAM is the number of nodes in the “actual” model.

A damage intensity metric, D , would also be useful and is defined as,

$$D = \frac{PDIM}{PDAM} \quad (5.6)$$

where, PDIM is the percent of damage simulated in the identification model and PDAM is the percent of damage imposed to the “actual” model.

Note that cases of $M > 1.0$ are not considered in this study. It is unrealistic for an identification model to be more “refined” than that of the actual structure. Recall that for all of Messina’s studies $M = 1$. All results presented herein implement an “actual” structure with 128 nodes (127 Euler-Bernoulli finite elements) and an imposed damage magnitude of 10 percent. The identification model size and damage magnitude are varied.

In this thesis damage is simulated by adding a lumped mass to a particular node of the FE model, and “10 percent damage” corresponds to a mass equivalent to 10 percent of the total beam mass. In Messina, Jones, and Williams’ study damage was simulated by stiffness reduction. It should be noted that these two different damage methods effect the natural frequencies of a structure differently¹. So, a separate generalized damage intensity parameter is established generalize Messina *et al.*’s results. As such, D^* , is defined as,

$$D^* = \frac{PSIM}{PSAM} \quad (5.7)$$

where, PSIM is the percent stiffness reduction simulated in the identification model and PSAM is the percent stiffness reduction imposed to the “actual” model.

This presents an opportunity to make another noteworthy point regarding the spatial truncation aspect of this study. In this work identification models of various refinements are implemented to determine the effect of spatial truncation on DLAC metric reliability, the accuracy of the natural frequencies obtained were not compromised using coarse FE models. For this simple structure note that the first four natural

¹Refer to Appendix C for an example and brief discussion.

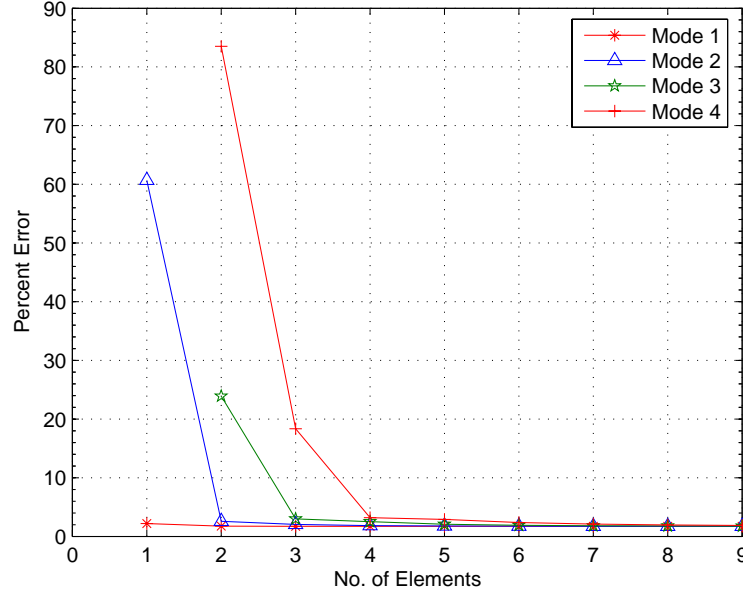


Figure 5.5: Finite Element Method and Exact ODE Solution Frequency Convergence

frequencies are within 2 percent of the exact solution with only a 4 element beam (5 node) model, cf. Figure 5.5.

5.4 The L_m Distance as a Sensitivity Metric

The L_m measure is the generalized distance between two points [3]. For the 2-dimensional case, the L_m distance between two points p_1 and p_2 at coordinates $[(x_1, y_1), (x_2, y_2)]$, respectively, would take the following form.

$$L_m = [|x_1 - x_2|^m + |y_1 - y_2|^m]^{\frac{1}{m}} \quad (5.8)$$

Perhaps in its more familiar form, when $m = 2$, the metric is known as the Euclidean distance, cf. Equation 5.9.

$$L_2 = \sqrt{(x_1 - x_2)^2 + (y_1 - y_2)^2} \quad (5.9)$$

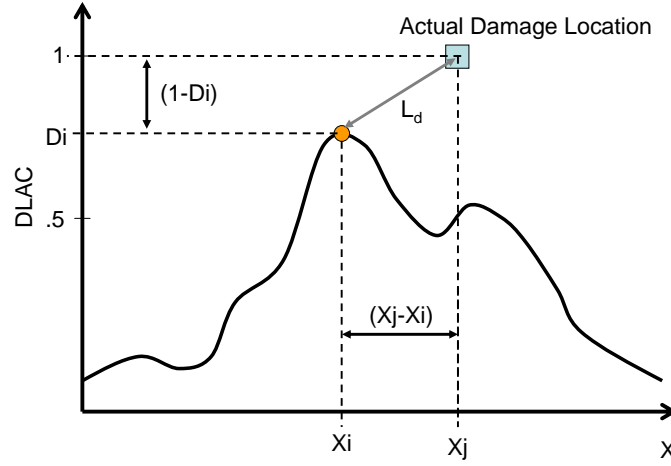


Figure 5.6: The L_d Performance Metric

In this study the L_2 , or Euclidean distance, metric is used as an error estimator to determine the error between that of the known damage location and the location and intensity of the maximum DLAC value, cf. Figure 5.6. Referred to in this study as the L_d metric, to distinguish it from any true spatial measure, the expression takes on the following form,

$$L_d = \sqrt{(x_j - x_i)^2 + (1 - D_i)^2} \quad (5.10)$$

where, $D_i = \max(\text{DLAC})$, $x_i = x(D_i)$, and x_j is the location where actual damage has been imposed. Note that a DLAC value of unity has been mandated at the actual damage location. As such, as $L_d \rightarrow 0$, damage is precisely localized.

5.4.1 DLAC Correlation Behavior

So that the reader might better appreciate the reliability analysis performed herein, some examples the DLAC correlation metric's behavior are presented, cf. Figure 5.7 and Figure 5.8.

Both example cases have “actual” structures consisting of 127 elements (10 percent damage) and an identification model of only 7 elements (1 percent damage), e.g. $M = .0625$, $D = 0.1$. Notice, the variation in the performance and how this effects the L_d metric. As such, when evaluating each possible damage scenario of the cantilever beam variations in the L_d metric are to be expected, cf. Figure 5.9. Notice the

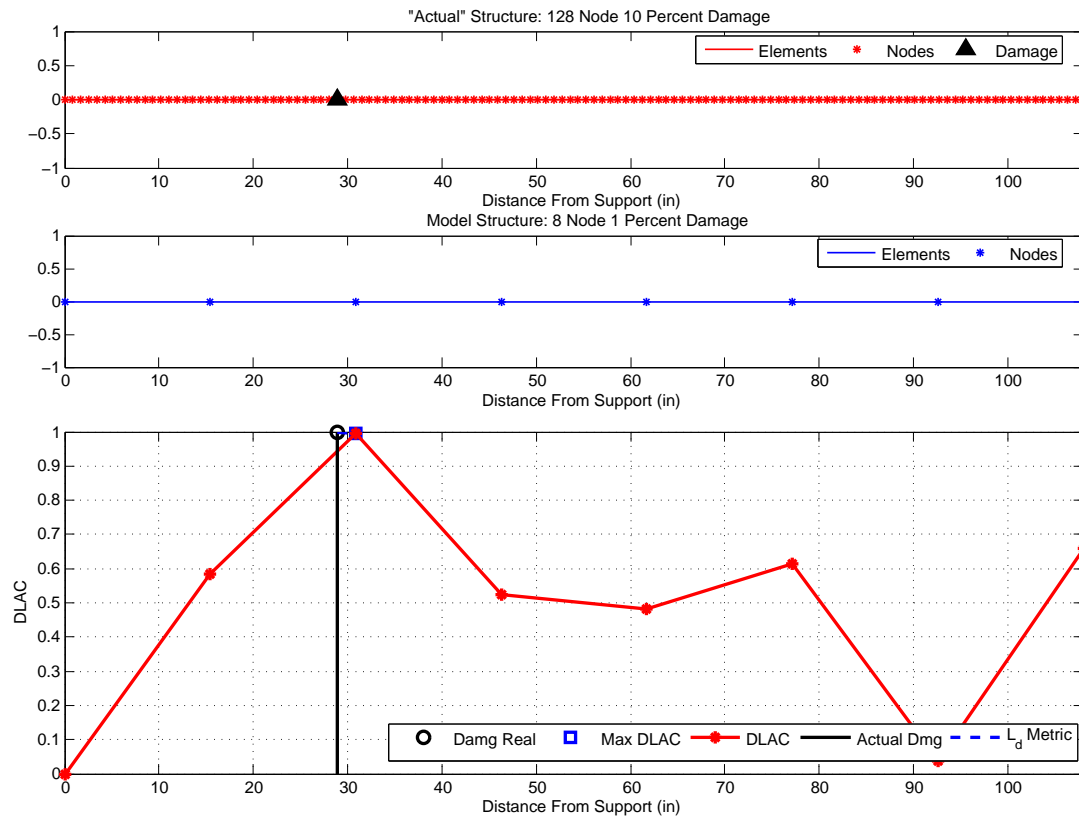


Figure 5.7: L_d Example of Good Localization

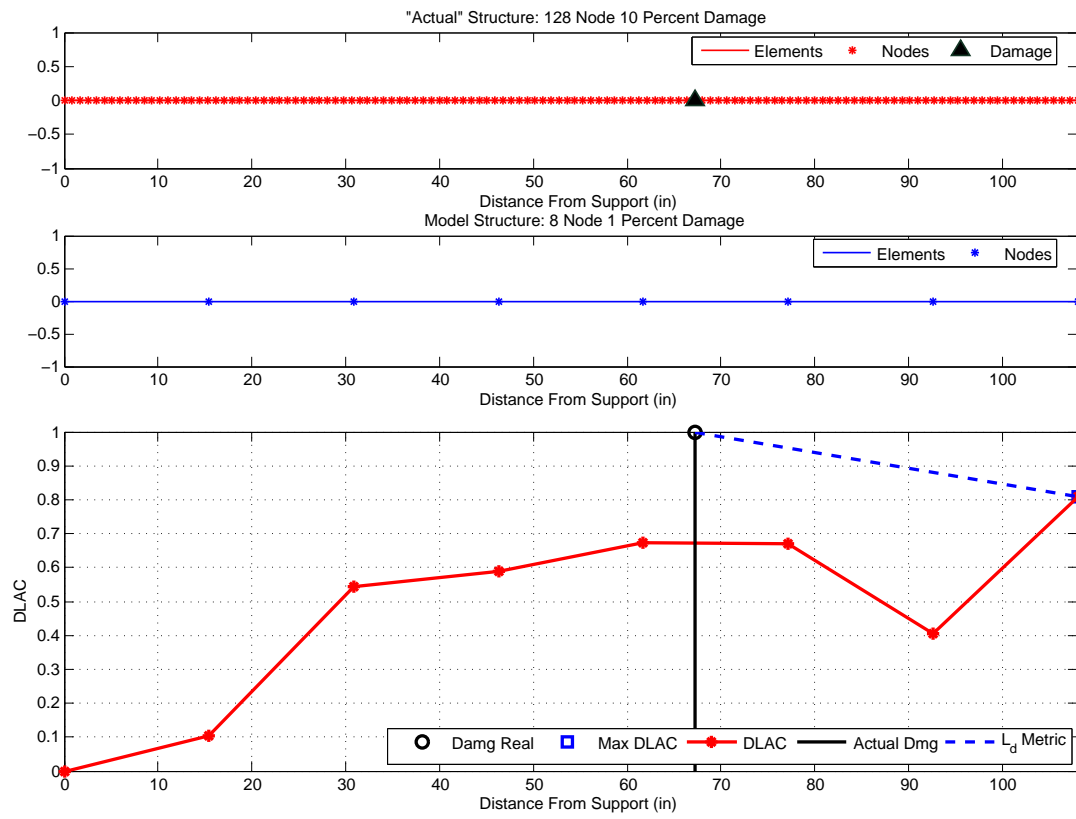


Figure 5.8: L_d Example of Poor Localization

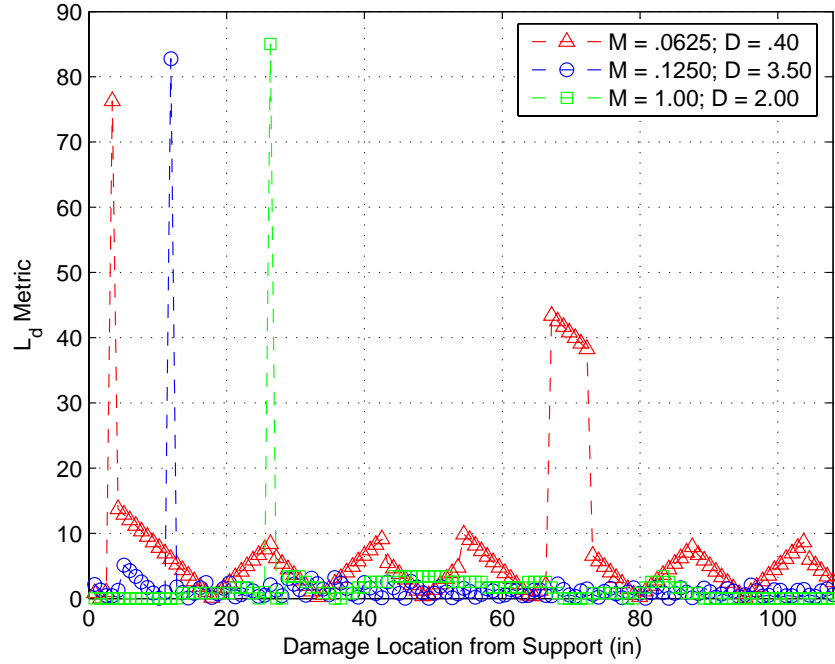


Figure 5.9: L_d vs. Damage Location (4 Modes)

presence of “spurts” in the L_d metric at certain damage locations. These spurts are present even when the model ratio is one. As such, this behavior should be accepted to be one of the natural shortcomings of a feature correlation-based technique.

5.4.2 Establishing the Success Criterion

To conduct a reliability analysis with the L_d performance metric a criterion for success must be established. As such, a prescribed maximum threshold for L_d can be set by the engineer who should take into consideration the refinement of the identification model.

In this study the success criterion was based on the AISC Load and Resistance Factor Design (LRFD) Manual’s specification for minimum bolt spacing, cf. Equation 5.11 [43]. (Assuming a structure with bolted connections.)

$$S = \frac{8}{3}d \quad (5.11)$$

Table 5.1: Average L_d Value: 4 Modes

M\D	0.10	0.40	1.00	1.50	2.00	3.50
0.063	6.43	6.96	6.91	6.56	6.58	6.17
0.125	<i>2.61</i>	<i>2.57</i>	<i>2.56</i>	<i>2.60</i>	<i>2.66</i>	2.99
0.250	<i>1.75</i>	<i>1.61</i>	<i>1.56</i>	<i>1.60</i>	<i>1.75</i>	<i>2.31</i>
0.500	<i>1.60</i>	<i>1.29</i>	<i>1.09</i>	<i>1.22</i>	<i>1.46</i>	<i>2.11</i>
1.000	<i>1.43</i>	<i>1.14</i>	<i>0.00</i>	<i>0.98</i>	<i>0.60</i>	<i>1.93</i>

S is the minimum spacing between bolts and d is the bolt diameter. Assuming bolts of no less than 1 inch diameter would be used to connect critical load bearing elements in large civil infrastructure a success criterion can be set using Equation 5.11. Realizing that $|1 - D_i| \ll 1$, typically, the condition for successful damage localization was set such that $L_d \leq 2.70$. This establishes a conservative localization threshold based on the minimum bolt hole spacing.

5.5 Sensitivity to Spatial Quantization

In Table 5.1 the average L_d value for various model ratios, M , and damage intensities, D , are presented. Notice the effect of spatial quantization has on the accuracy of the DLAC localization method. Values which are within the limits of the success criterion are denoted by *italics*. When $M = 0.063$, the model is much too coarse to attain localization values within the success criterion limit imposed for all values of D . Notice that when $M = 0.125$, despite distances between each node being greater than the success rate criterion, 6.75 inches on center, the DLAC procedure can capture results within the threshold for nearly all values of D . Of course, the as the model ratio approaches unity, the average L_d value continues to decrease. These uncorrupted results, i.e. no noise addition, indicate that spatial quantization should be considered when implementing the DLAC method.

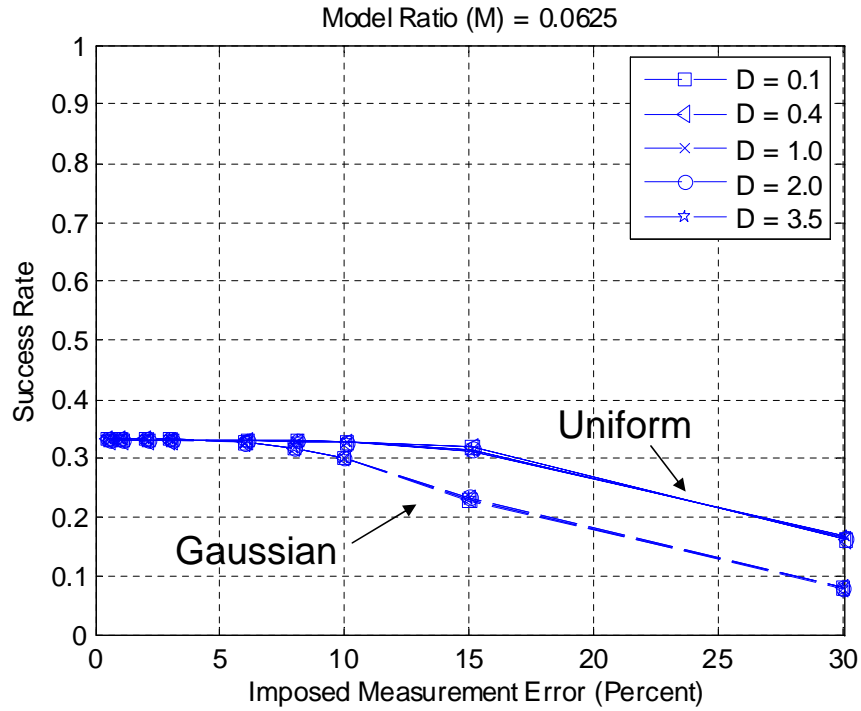


Figure 5.10: DLAC Quantization Performance Noise: M = .0625, 4 Modes

5.6 Measurement Noise

To simulate “actual” natural frequencies, the identification model’s frequencies are seeded with noise according to Equation 5.1. Since the distribution of errors produced by a fractional polynomial curve-fitting technique are unknown the effects of both uniform and Gaussian distributions of noise are implemented. The range of the uniform distribution is -1 to +1. The Gaussian distribution has a zero mean and standard deviation of one. Success rates were determined from 50 trials. To consistently compare results from all tests 50 sets of 30 random numbers (for each distribution) were generated in MATLAB and stored. As such, the same random numbers were used for each different test conducted. Histograms of the 50 sets of each type of noise used in the study are presented in Appendix D.

The effect of the amplitude and distribution of measurement noise are presented in Figure 5.10, Figure 5.11, Figure 5.12, Figure 5.13, and Figure 5.14.

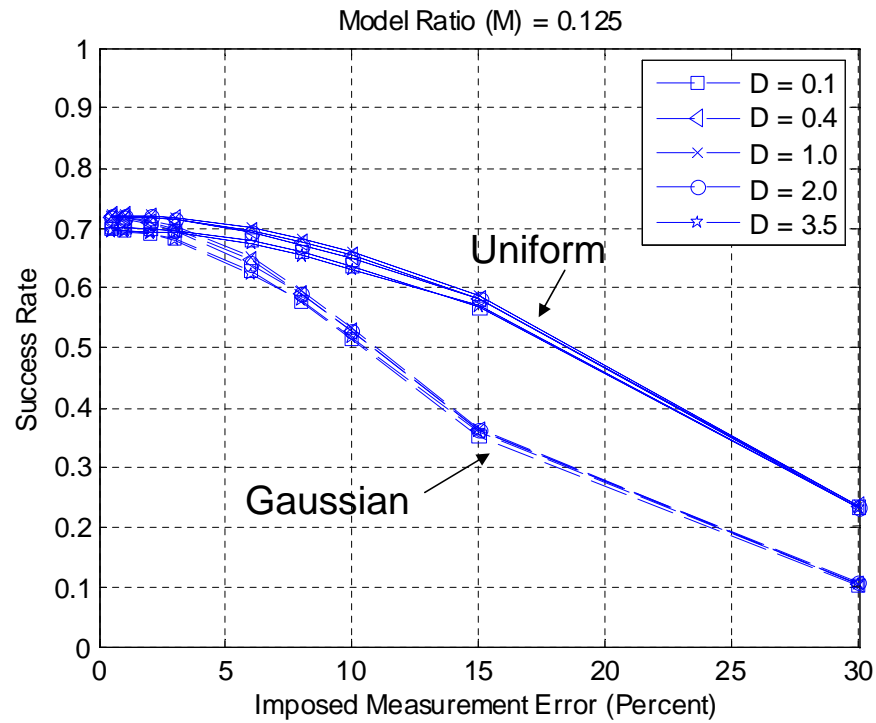


Figure 5.11: DLAC Quantization Performance Noise: $M = .1250$, 4 Modes

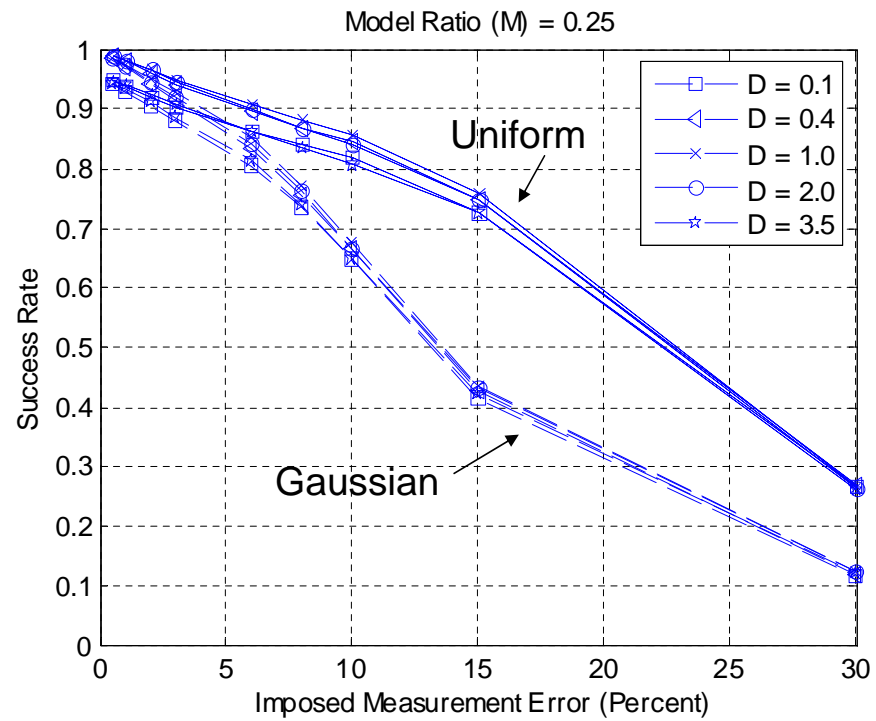


Figure 5.12: DLAC Quantization Performance Noise: $M = .2500$, 4 Modes

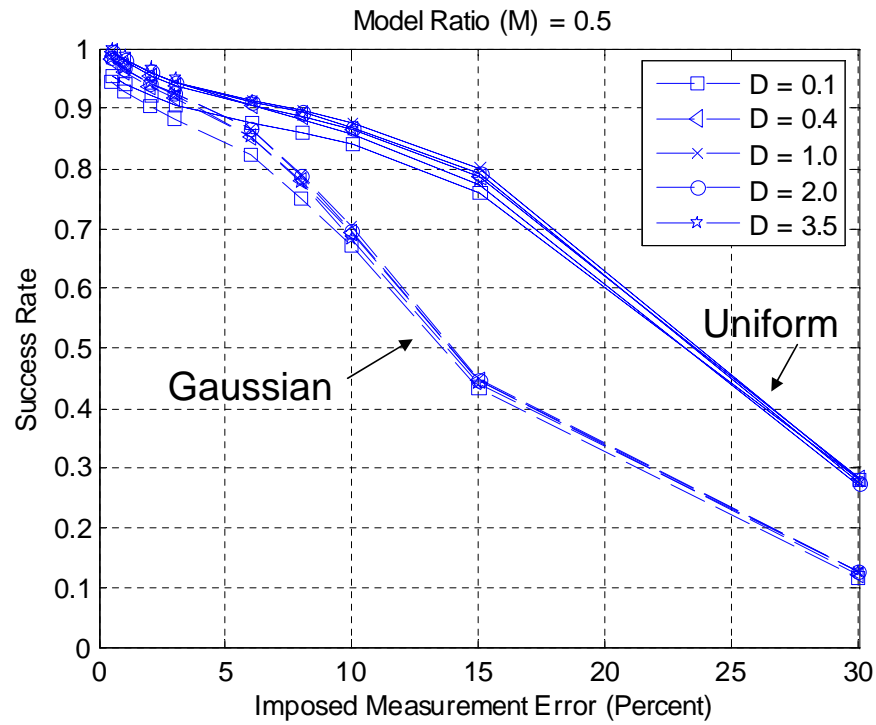


Figure 5.13: DLAC Quantization Performance Noise: M = .5000, 4 Modes

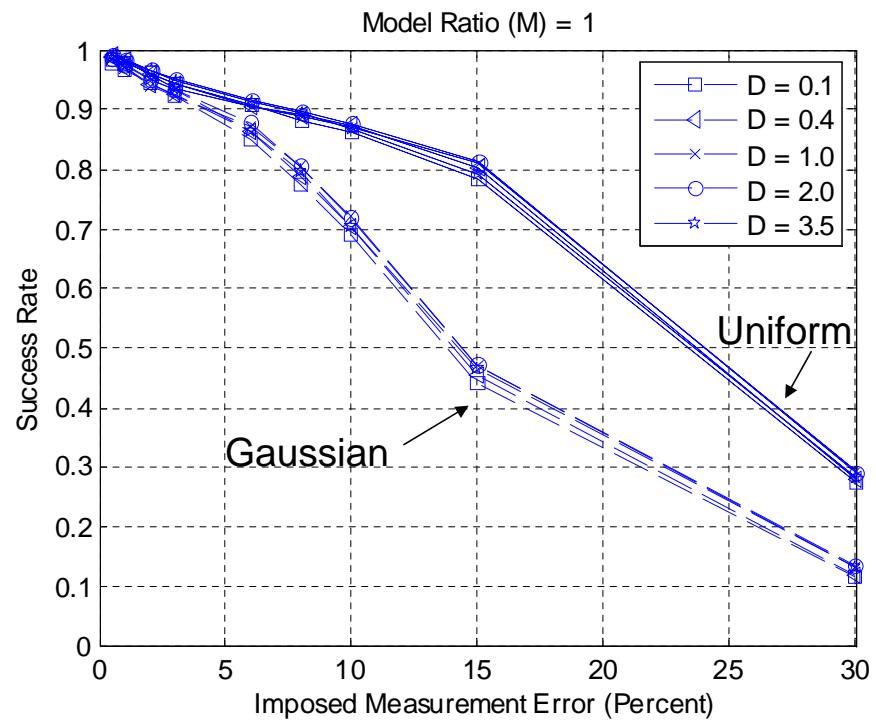


Figure 5.14: DLAC Quantization Performance Noise: M = 1.000

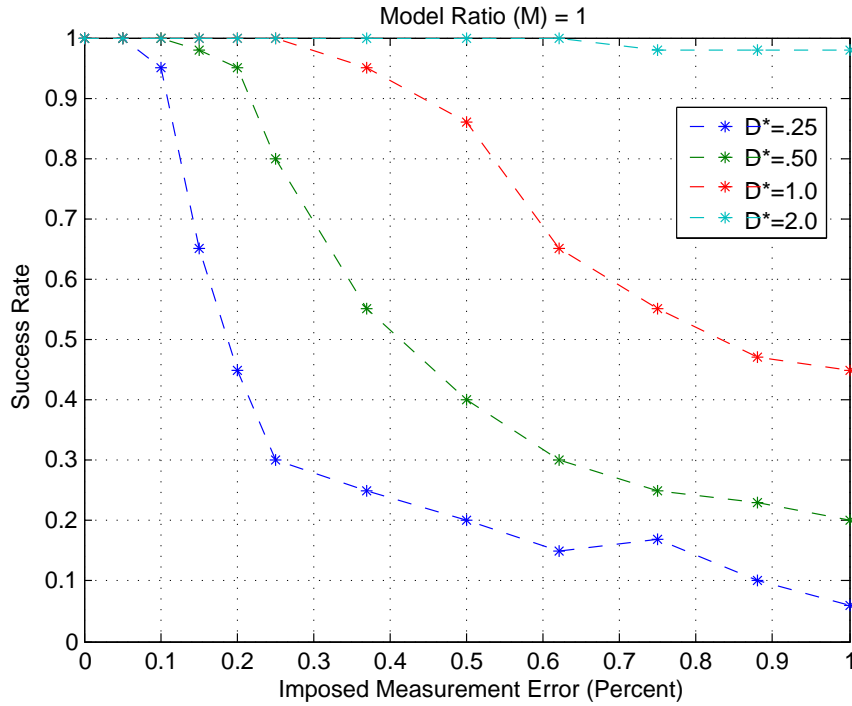


Figure 5.15: Measurement Noise: $M = 1.000$, 20 Modes [38]

Note that all values of damage ratio, D , performed similarly. Notice that once the amplitude of noise reaches approximately 3 percent, the effects of noise distribution becomes noticeable for all values of D . In all cases, after this threshold is reached, the Gaussian noise reduces the DLAC success rate. This reduction is drastic at times, nearly as much as a 50 percent difference in success rates calculated with uniform noise, Figure 5.13 at 15 percent imposed measurement error. Uniformly distributed noise effects the performance with much less severity once the 3 percent error threshold is crossed. Since actual noise characteristics are unknown perhaps reasonable estimate of the performance of the DLAC localization metric can be found within the area enclosed by uniform and Gaussian reliability estimates.

Now, consider the results without spatial quantization, presented by Messina *et al.* (1996), cf. Figure 5.15. Notice that these results are much more sensitive to the addition of noise, the maximum level of imposed error is 1 percent, and that localization successes are highly dependant upon the amount the damage ratio, D^* . This is quite a drastic difference between the results presented in Figure 5.10, Figure 5.11,

Table 5.2: Average L_d Value: 5 Modes

M\D	0.10	0.40	1.00	1.50	2.00	3.50
0.063	6.25	6.18	5.89	5.90	5.93	5.76
0.125	<i>2.30</i>	<i>1.93</i>	<i>1.93</i>	<i>1.96</i>	<i>2.00</i>	<i>2.13</i>
0.250	<i>1.08</i>	<i>0.97</i>	<i>0.89</i>	<i>0.95</i>	<i>1.01</i>	<i>1.41</i>
0.500	<i>0.79</i>	<i>0.62</i>	<i>0.43</i>	<i>0.52</i>	<i>0.66</i>	<i>1.14</i>
1.000	<i>0.55</i>	<i>0.30</i>	<i>0.00</i>	<i>0.24</i>	<i>0.44</i>	<i>0.97</i>

Figure 5.12, Figure 5.13, and Figure 5.14. This is one reason why this researcher feels that noise was inappropriately used to generate the “actual” system parameters.

5.7 Modal Truncation

Consider the uncorrupted results presented in Table 5.2 in which five natural frequencies were used in the correlation procedure. Again, values which are within the limits of the success criterion are listed in *italics*.

Notice the reduction in average L_d value. Now consider the modal truncation results with Gaussian noise, cf. Figure 5.16, Figure 5.17, Figure 5.18, and Figure 5.19.

Note, here again all values of damage ratio, D , performed in similar fashion. Only Gaussian noise needs to be implemented to establish a conservative estimate of the reliability of the DLAC localization procedure. Notice as the number of natural frequencies used in the correlation is increased from 1 to 15, the success rate increases from approximately 0.5 percent to 60 percent with an imposed damage intensity of 15 percent. This noise level is a fairly “strong” amplitude of measurement noise, and it seems unlikely that this amount would be observed in practice. What is valuable to note here is the rate at which the reliability improves as additional modal frequencies of the structure are considered. From 1 to 3 modes, the rate increasing a sharp rate. However, from 3 to 5 modes the rate decreases somewhat and appears to continues decrease from there on. Ultimately for cases when $M = .25$, 0.5, and 1.0 the results appear to converge to a 62 percent success rate, cf. Figure 5.17, Figure 5.18, and Figure 5.19. When $M = 0.125$, the model does not appear to be refined enough to

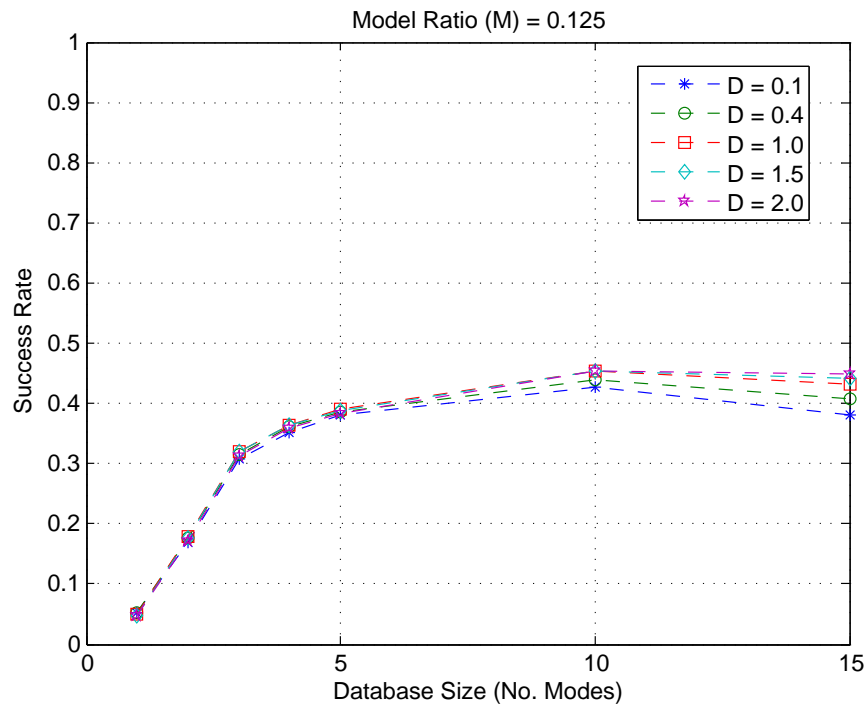


Figure 5.16: DLAC Truncation Performance: 15% Gaussian Noise, $M = 0.125$

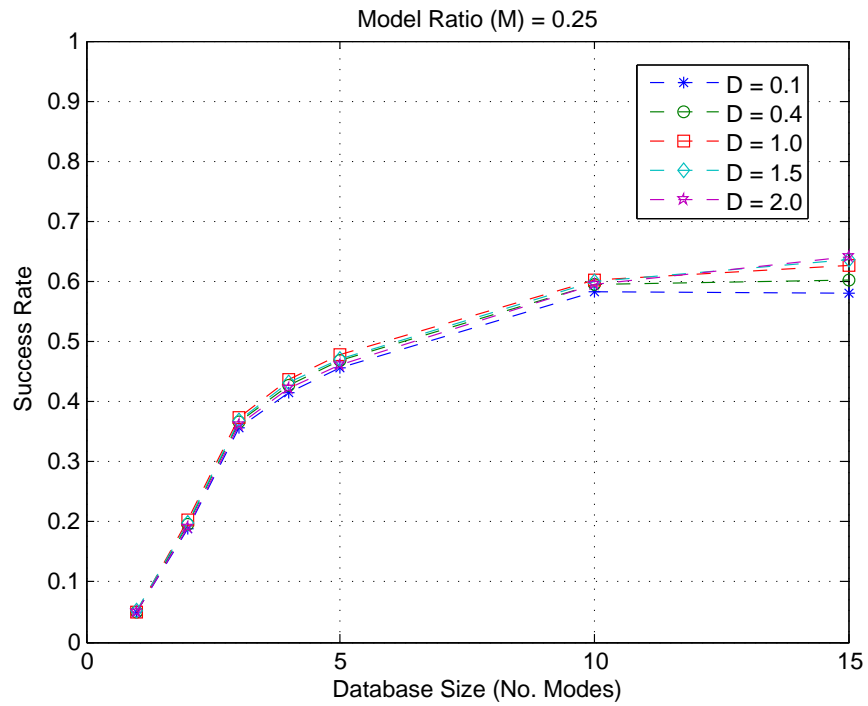


Figure 5.17: DLAC Truncation Performance: 15% Gaussian Noise, $M = 0.250$

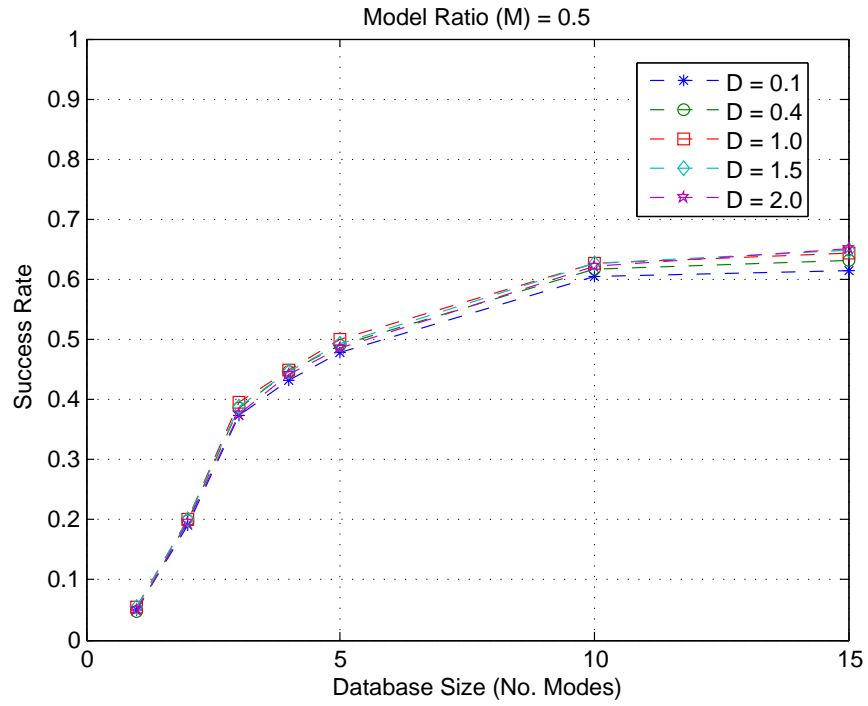


Figure 5.18: DLAC Truncation Performance: 15% Gaussian Noise, $M = 0.500$

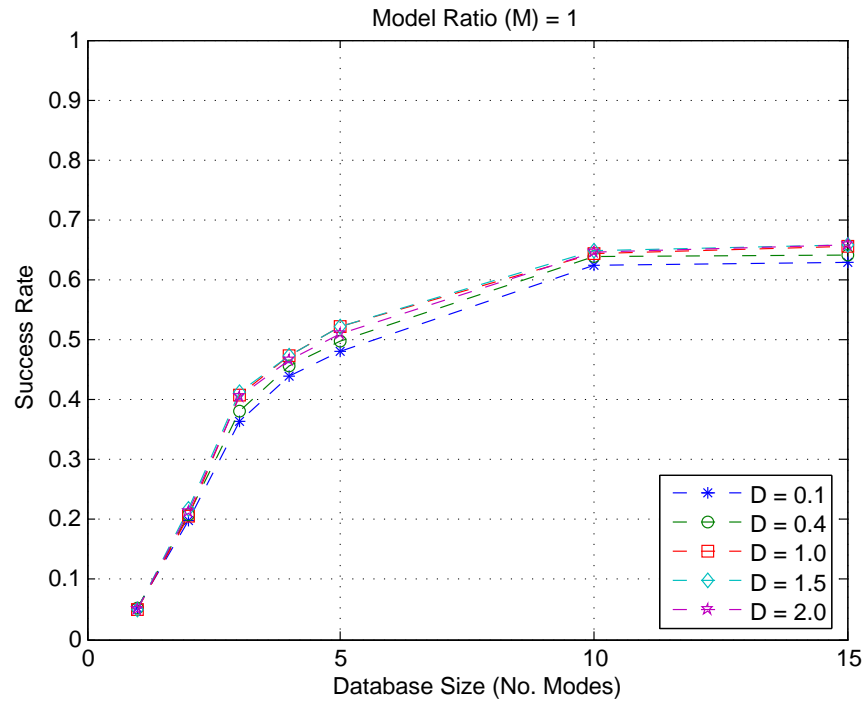


Figure 5.19: DLAC Truncation Performance: 15% Gaussian Noise, $M = 1.000$

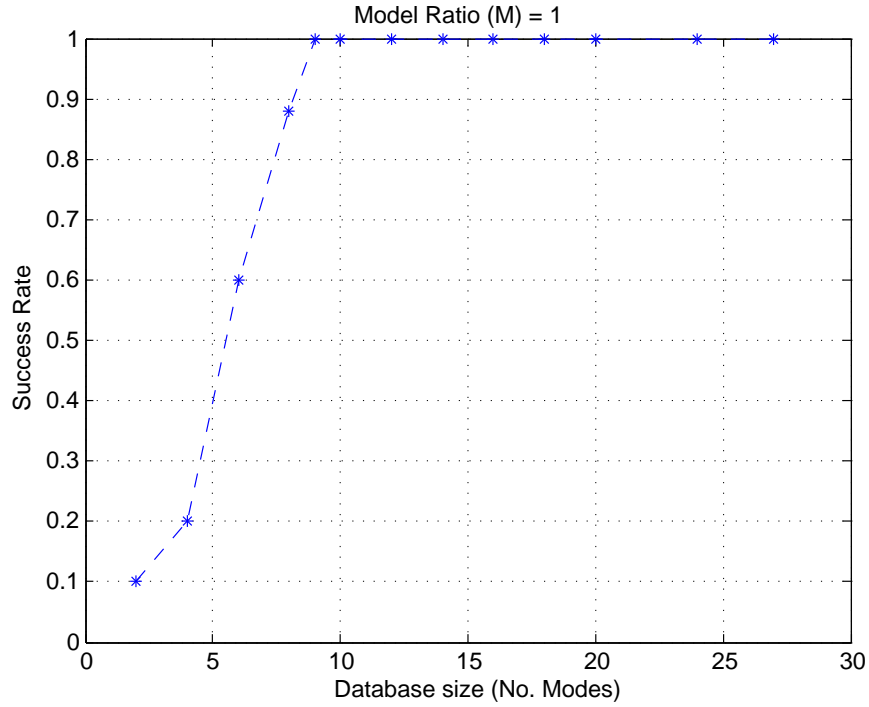


Figure 5.20: Modal Truncation: 15% Uniform Noise, $M = 1.000$, $D^* = 1.000$, [38]

localize damage with the amplitude of imposed measurement errors, cf. Figure 5.16. Interestingly, the $M = 0.125$, identification model initially exhibits the same success rate trend as the more refined models; however, the results ultimately converge to a 45 percent success rate.

Messina *et al.* also considered the effects of modal truncation in their analysis, cf. Figure 5.7. In the results they presented despite using a very low amplitude of uniform noise the general trend is similar to those observed in this study. For example, the number of modes at which the success rates tend to converge is approximately the same, at 10 modes.

5.8 Summary

The results of this study indicate that features such as spatial quantization and distribution of the imposed measurement noise do effect the reliability of the DLAC localization method.

Identification model quantization, in this study, appears to significantly effect the reliability of the method if model ratios of less than $M = 0.25$ are implemented. In all cases, the reliability of the method appeared insensitive to the damage ratio, D . Characteristic distribution of the noise implemented to simulate “actual” modal parameters greatly affect the sensitivity of the DLAC metric after a threshold of 3 percent was crossed. In one case the reliability of the DLAC method was reduced the by nearly 50 percent, cf. Figure 5.13 (15 percent imposed error).

Admittedly Messina, Jones, and Williams implemented their study on a slightly more complex structure, geometrically speaking. Thus, perhaps to truly understand the effects of the considerations taken in this study, Messina’s structure should be re-analyzed under the same conditions. Such a comparison would be useful.

In summary, implementing the L_d performance metric and a reasonable condition on which to base success, the DLAC procedure has been shown to be reliable for localization of single damage scenarios in a cantilever beam model.

Chapter 6

Conclusion and Future Work

6.1 Conclusions

In Chapter 1 an overview of the advantages of a vibration-based structural health monitoring scheme for civil infrastructure was presented. However, despite the advantages of a vibration-based SHM paradigm presently the traditional wired sensors and centralized data acquisition systems, i.e. monitoring equipment, is too expensive for widespread application. As such, for vibration-based SHM technology to become a practical alternative to visual inspection of civil structures these large capital costs must be reduced. Recently, with the development of inexpensive motes and MEMS sensor/actuator technology which can be used in place of traditional monitoring equipment vibration-based SHM is becoming feasible financially. Presently, strides are being made to overcome the intrinsic limitations associated with any wireless battery powered device. As such, to work within these limitations it is the job of the structural engineer to develop health monitoring paradigms that can function autonomously in a distributed processing fashion.

In Chapter 2 both theoretical and applied working principles behind vibration-based health monitoring were presented in the context of a single degree-of-freedom system. A computationally efficient curve-fitting technique was re-introduced as a method for automatically extracting the natural frequencies from a structure's response power spectrum (PSD). Having been developed during an age of limited computational power, i.e. 1959, this method appears to be well suited for the implementation of decentralized SHM methods.

In Chapter 3 a feature correlation-based health monitoring paradigm was proposed for a distributed processing environment. The Damage Location Assurance Criterion (DLAC) single damage localization methodology developed by Messina *et al.* (1996) was selected as the basis of the detection algorithm. Since the DLAC metric is a natural frequency correlation-based method, multiple channels of data are not required for implementation. As such, with the availability of reliable automated frequency extraction algorithms this method was deemed suitable for implementation on a smart wireless sensor platform.

In Chapter 4 the proposed distributed vibration-based SHM algorithm was experimentally tested offline. Two proof-of-concept damage localization experiments were conducted on two different laboratory test structures. Data was acquired with Mica2 and MicaZ mote systems which employ MEMS technology accelerometers. Since the data processing capabilities of the Mica motes has not yet reached the level of sophistication needed to perform onboard power spectrum estimates, all data was processed offline in a fashion consistent to the embedded operation of the algorithm. The results indicate that damage can be localized using mote hardware and the proposed algorithm.

In Chapter 5 a sensitivity study of the DLAC metric and localization procedure was performed. While Messina *et al.* conducted a similar study in their original 1996 work it, perhaps, failed to evaluate the effects of certain realistic hurdles which emerge during actual implementation of the method. As such, more realistic reliability assessment of the DLAC numerical study is thought to have been performed. The results from this second study indicate the DLAC procedure is robust and that reliable single damage localization can be made using this technique. However, the reliability of this method is greatly effected by the distribution of the system noise and the refinement of the identification model implemented.

In summary, the following contributions were made through the work discussed in this thesis. A viable vibration-based SHM algorithm for a distributed smart sensor network was developed and validated in an “offline” mode. A possible monitoring framework for implementation of this algorithm on a structure was also presented. The current state-of-the-art performance capabilities of commercially available motes with MEMS technology sensors were examined during two full-scale experimental

studies. A new sensitivity analysis of the DLAC method was performed considering the effects of three realistic implementation issues, spatial quantization, modal truncation, and noise distribution.

6.2 Future Works

There are, of course, a multitude of paths which fork from the culmination of the work presented in this thesis. However, a few suggestions will now be made to help others in this field pursue those avenues which appear to be most promising.

The proposed SHM algorithm presented was validated experimentally in an offline fashion which simulated the embedded operation of the system. Clearly, a future study should be conducted with the algorithm fully embedded on a SWS platform and experimentally validated in a true online fashion. The results of this future work should then be compared to other monitoring techniques which can be decentralized and embedded on SWSs.

Feature correlation-based health monitoring is a robust concept on which to perform distributed SHM implementing SWSN. However, a notable setback in the formulation of many feature correlation-based SHM methodologies, including the DLAC, is computational power required to generate the damaged feature database. If explicit methods are used to generate the database, i.e. those which do not involve Genetic Algorithms (GA) or statistical approaches, for a typical civil structure, this can be too computationally intensive for even a PC, not to mention a SWS. (Thus, to reduce the computational requirements in this study an algorithm which is only capable of detecting single damage scenarios is evaluated.) Methods which make approximations when generating the feature database, i.e. GA and statistical analysis, offer improvements, but they do not appear to be implementable in the near-term due to the limited computational power currently available on a SWS.

The emergence of artificial neural networks which implement statistical analysis, called probabilistic neural networks (PNN), offer new insight into facing these limitations. These methods appear to be very efficient at localizing damage accurately in complex structures [29]. As a result of their efficiency, PNN's might be able to

address the occurrence of multiple simultaneous damage sites which were not considered in this study. As such, this researcher feels that the development of PNN algorithms which could be embedded on a SWS will be a step closer to bringing full-scale implementation of an SHM technology to fruition.

Appendix A

Mote Developments

UC Berkeley-Crossbow WpC (1999)							UC Berkeley-Crossbow MICA (2002)		UC Berkeley-Crossbow MICA2 (2003)		Intel iMote, Kling (2003)		Microstrain, Galbreath <i>et al.</i> (2003)		Rockwell-Agre <i>et al.</i> (1999)			
DATA ACQUISITION SPECIFICATIONS																		
A/D Channels							8		8				8		4			
Sample Rate							1 kHz		1 kHz				1.7 kHz (one channel)		400 Hz			
A/D Resolution							10-bit		10-bit				12-bit		20-bit			
Digital Inputs																		
EMBEDDED COMPUTING SPECIFICATIONS																		
Processor							Atmel AT90LS8535		Atmel ATmega163L		Atmel ATmega128L		Zeevo ARM7TDMI		MicroChip PIC16F877		Intel StrongARM 1100	
Bus Size							8-bit		8-bit		8-bit		32-bit		8-bit		32-bit	
Clock Speed							4 MHz		4 MHz		7.383 MHz		12 MHz		133 MHz		133 MHz	
Program Memory							8 kB		16 kB		128 kB		64 kB		1 MB		1 MB	
Data Memory							32 kB		32 kB		512 kB		512 kB		2 MB		128 kB	
WIRELESS CHANNEL SPECIFICATIONS																		
Radio							TR1000		TR1000		Chipcon CC1000		Wireless BT Zeevo		RF Monolithics DR-3000-1		Conexant RDSSSM	
Frequency Band							868 / 916 MHz		868 / 916 MHz		315, 433, or 868 / 916MHz		2.4 GHz		916.5 MHz		916 MHz	
Wireless Standard							No		No		Yes (Software)		IEEE 802.11b				Yes	
Spread Spectrum													Yes					
Outdoor Range																		
Enclosed Range																		
Data Rate							10 kbps		40 kbps		38.4 kbps		600 kbps		75 kbps		100 m 100 kbps	
FINAL ASSEMBLED UNIT ATTRIBUTES																		
Dimensions							2.5 x 2.5 x 1.3 cm										7.3 x 7.3 x 8.9 cm	
Power							575 mAh		2850 mAh		1000 mAh		Battery		Battery (3.6V)		Battery (two 9V)	
Power Source							Coin Cell		Battery (3V)		Coin Cell							

Straser & Kiremidjian (1998)		Bennett <i>et al.</i> (1999)	Lynch <i>et al.</i> (2001, 2002a, 2002b)	Mitchell, Rao, and Pottinger (2002)	Kottapalli <i>et al.</i> (2003)	Lynch, <i>et al.</i> (2003, 2004a, 2004b)	Aoki, Fujino, and Abe (2003)	Basheer, Rao, and Derriso (2003)
DATA ACQUISITION SPECIFICATIONS								
A/D Channels	8	4	1	5	1	Multiple		
Sample Rate	240 Hz		100 kHz	20 MHz	20 MHz	100 kHz		
A/D Resolution	16-bit	16-bit	16-bit	16-bit	8-bit	16-bit		
Digital Inputs	0		2	0	0	2		
EMBEDDED COMPUTING SPECIFICATIONS								
Processor	Motorola 68HC11	Hitachi H8/329	Atmel AVR8515	Cygnal 8051	Microchip PIC16F73	Atmel AT90S8515	Renesas H8/4069F	ARM7TDMI
Bus Size	8-bit	8-bit	8-bit		8-bit	8-bit/32-bit	8-bit	32-bit
Clock Speed	2.1 MHz	4.9 Hz	4 MHz		20 MHz	4 MHz/20 MHz	20 MHz	
Program Memory	16 kB	32 kB	8 kB	2 kB	4 kB	8 kB/26 kB	128 kB	
Data Memory	32 kB		32 kB	128 kB	192 kB	512 kB/448 kB	2 Mb	
WIRELESS CHANNEL SPECIFICATIONS								
Radio	Proxim ProxLink	Radiometrix	Proxim Rangelan2	Ericsson Bluetooth	BlueChip RBF915	Proxim Rangelan2	Realtek RTL-8019AS	Phillips Blueberry Bluetooth
Frequency Band	900 MHz	418 MHz	2.4 GHz	2.4 GHz	900 MHz	2.4 GHz		IEEE 802.11b
Wireless Standard	Yes		Yes	IEEE 802.11b	Yes	Yes	50 m	Yes
Spread Spectrum	300 m	300 m	300 m	10 m	500 m	300 m	50 m	100 m
Outdoor Range	150 m		150 m	10 m	200 m	150 m	50 m	
Enclosed Range	19.2 kbps	40 kbps	1.6 Mbps		10 kbps	1.6 Mbps		
Data Rate								
FINAL ASSEMBLED UNIT ATTRIBUTES								
Dimensions	15x13x10 cm	15D x 30 cm	10x10x5 cm	5x3.8x1.2 cm	10x5x1.5 cm	12x10x2 cm	30x6x8 cm	2.5x2.5x2.5 cm
Power				120 mW	100 mW			
Power Source	Battery (9V)	Battery (6V)	Battery (9V)	Battery	Battery (9V)	Battery (9V)		Battery

Figure A.2: Academic Smart Wireless Sensing Units (1998–2003) [33]

Casciati, <i>et al.</i> (2003b, 2004) Wang <i>et al.</i> (2003, 2004) & Cu <i>et al.</i> (2004) Mastroiolo <i>et al.</i> (2004) & Chung <i>et al.</i> (2004) Shinozuka (2003) & Ou, Li & Yu (2004) Sazanov, Janoyan, Farrar <i>et al.</i> (2005) & Allen (2005) Wang, Lynch & Law (2005) Pei <i>et al.</i> (2005)									
DATA ACQUISITION SPECIFICATIONS									
A/D Channels	8	8	5	4/2	6	6	4		
Sample Rate		> 50 Hz	480 Hz			200 kHz	100 kHz		100/500 Hz
A/D Resolution	12-bit	12-bit	16-bit	8-bit / 10-bit	12-bit	16-bit	16-bit		10/12/16-bit
Digital Inputs		multiple	0	2	16		0		
EMBEDDED COMPUTING SPECIFICATIONS									
Processor		Analog Devices ADuC832	Microchip PICmicro 16-bit / 8-bit	Atmel AVR ATmega 8L	Texas Instruments MSP430F1611	Intel Pentium / Motorola	Atmel AVR ATmega128		Motorola 68HC11
Bus Size		8-bit		8-bit		16-bit	8-bit		
Clock Speed						120/233 MHz	8 MHz		
Program Memory		62 kB		8 kB	16 Mb	256 MB	128 kB		32 kB
Data Memory		2 kB		1 kB		Compact Flash	128 kB		32 kB
WIRELESS CHANNEL SPECIFICATIONS									
Radio	Aurel XTR-915	Linx Technologies	BlueChip RFB915B	Chipcon CC1000	Chipcon CC2420	Motorola neuRFon	Maxstream 9XCite		MaxStream Xstream
Frequency Band	914.5 MHz	916 MHz	900 MHz	433 MHz	2.4 GHz	2.4 GHz	900 MHz		900 MHz/2.4 GHz
Wireless Standard									
Spread Spectrum	No	No	Yes	Yes (Software)	IEEE 802.15.4	IEEE 802.15.4	Yes	Yes	Yes
Outdoor Range		152 m	200-300 m		75 m	9.1 m	300 m		
Enclosed Range		61 m				9.1 m	100 m		
Data Rate	100 kbps	33.6 kbps	19.2 kbps	76.8 kbps	250 kbps	230 kbps	38.4 kbps		
FINAL ASSEMBLED UNIT ATTRIBUTES									
Dimensions			8x8x2 cm		6x9x3.1 cm		10x6x4 cm		
Power									
Power Source		Battery		Battery	75 mW	6 W	Battery (7.5V)		Battery (9V)

Figure A.3: Academic Smart Wireless Sensing Units (2003–2005) [33]

Appendix B

ADXL202E MEMS Accelerometer

All of the studies presented in this work examine acceleration time histories of structures to localize potential damage. The performance of the sensor used to gather this data greatly effects the accuracy of the features obtained. In all of the studies presented in this work the ADXL202E MEMS accelerometer sensor was implemented. The sensor itself is a high quality instrument, although special considerations need to be taken when configuring the device for operation on a mote.

The ADXL202E is a low-cost, low-power complete dual-axis MEMS accelerometer with a digital output [1]. Each of sensing elements consists of a polysilicon mass-spring system and uses a differential capacitor to produce an analog signal proportional to accelerations experienced by the proof the mass. While the sensors themselves remain linear through 6 kHz, the onboard ADC does not sample sufficiently fast enough to accurately capture the analog signal. As such, to enhance the accuracy of the digital output the analog sensor bandwidth must be low-pass filtered (decreased) before it is digitized.

To digitize the analog sensor signal onboard the ADXL202E an analog-to-duty cycle modulator and microprocessor counter have been integrated into the circuit. The analog to duty-cycle converter (ADC) has approximately a 14-bit resolution and is preconfigured to sample at a rate of 1 kHz [1]. Taking into consideration the Nyquist Sampling Theorem ¹ to ensure the signal is not aliased, the ADC can effectively acquire signals up to a frequency of 500 Hz. The ADXL202E has a primary low-pass filter, $R_{\text{flt}} = 32\text{k}\Omega$, which discards frequencies above 5 kHz, cf. Figure B.1. The

¹A signal that is bandlimited between $[-B, B]$ can be recovered from its samples taken every $.5/B$ seconds.

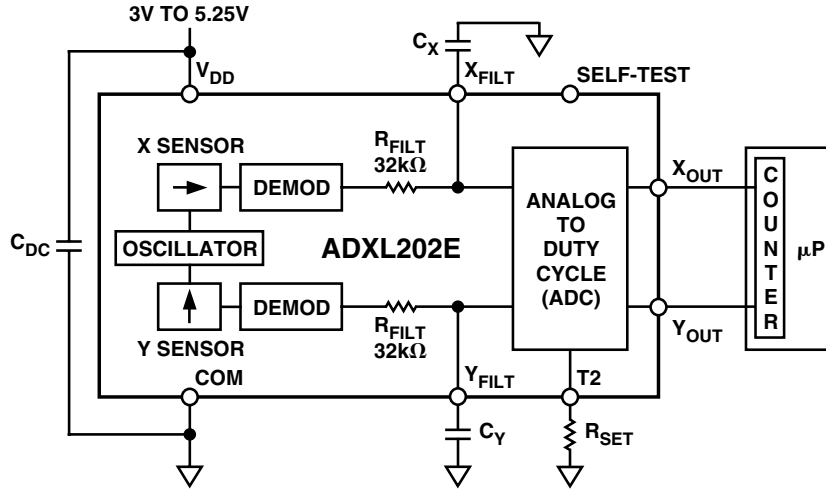


Figure B.1: Functional Block Diagram: ADXL202E MEMS Accelerometer [1]

bandwidth may be further modified by the user by installing external capacitors at the C_X and C_Y prongs, cf. Figure B.1. Interestingly this secondary low-pass filter comes configured from the manufacturer with a redundant bandwidth of 5 kHz. As such, the manufactured configuration of the ADC sampling rate and the filtered analog sensor bandwidth are mismatched and the ADXL202E digital signal is aliased, insensitive, and has poor resolution. However, this can be fixed by adding a 0.10, 0.05, or 0.027 μF capacitor at C_X and C_Y pins, cf. Figure B.1. This would reduce the analog signal bandwidth to 50, 100, 200 Hz, respectively, before being digitized [1]

On the MTS310CA multi-sensorboard manufactured by Crossbow for their Mica series mote the ADXL202E accelerometer's analog output is accessed from external pins, (after X_{filt} and Y_{filt} on Figure B.1). This avoids issues with the analog to duty-cycle modulator, since this hardware is bypassed. According to the MTS310A user's manual the bandwidth of the accelerometer's analog signal is set to 50 Hz, though it is uncertain if filtering was done at the C_X and C_Y pins on the ADXL202E or using hardware onboard the Mica mote. Nevertheless, the analog signal is quantized with the Mica mote's 10-bit analog-to-digital converter. However, the voltage is not conditioned properly and full-scale use of the 10-bit ADC is not achieved. In order to make use of the full range of the ADC onboard the Mica motes an operational amplifier could be used to correctly scale the output voltage.

On Intel’s iMote accelerometer sensorboard the digital output is accessed. However, all filter settings are left in the as manufactured state, i.e. 5 kHz bandwidth. As such, with the 1 kHz sampling rate of the onboard ADC, low sensitivity, poor resolution, and aliasing all become problems. It is not by any means very well suited to low amplitude and frequency vibration monitoring.

In this work it has been found that when the ADXL202E has been prefabricated onto proprietary sensorboards, the sensor’s performance has inadvertently been reduced. The implementation issues associated with these “turn-key” sensorboards have been corroborated by other researchers too [26, 49].

Appendix C

Damage Simulation and its Effects on W_n

At times in this work damage has been simulated by imposing a mass change to the system. While a loss of stiffness is certainly the realistic means which actual structures suffer damage, it is less costly to impose mass increases and than that of stiffness reductions for laboratory experiments involving continuous parameter systems. (With a truss structure or lumped parameter system, it is not expensive to simulate damage by stiffness reduction as *pre-damaged* elements may be substituted in and out of the system [8].) As such, it is of interest to realize the potential effects simulating damage by way of mass change may have on the features being monitored.

In this study the features extracted from structural response behavior were natural frequencies. Consider the equation governing the natural frequency of a single degree-of-freedom system, cf. Equation C.1.

$$\omega_n(k, m) = \sqrt{\frac{k}{m}} \quad (\text{C.1})$$

By inspection of Equation C.1, it is clear that two different nonlinear relationships describe the natural frequency of a system, depending on which parameter k or m is varied. If mass, m , is held constant, then $\omega_n(k)$ varies according to \sqrt{k} . If stiffness, k , is held constant, then $\omega_n(m)$ varies according to $\sqrt{\frac{1}{m}}$.

The result of simulating damage by either mass or stiffness and its effect on the natural frequency of a single degree-of-freedom system has been presented in Figure C.1.

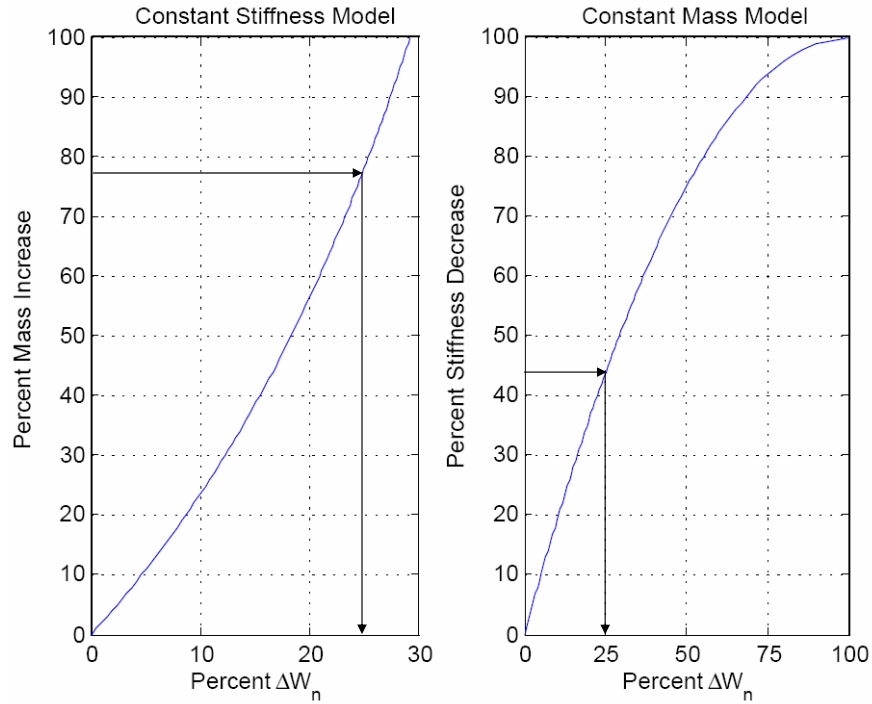


Figure C.1: Nonlinear ω_n Relation (SDOF)

Notice that to achieve 25 percent change in natural frequency a 78 percent increase in mass is required. Yet to achieve a 25 percent change in natural frequency by way of stiffness a 44 percent reduction must be imposed to the system. As such, when simulating damage in two identical structures, one which damage is simulated by mass addition and the other by stiffness reduction, one must consider the amount by which the feature being monitored is changing to maintain consistency. This concept may be generalized to multi-degree-of-freedom systems.

Appendix D

Additional Figures

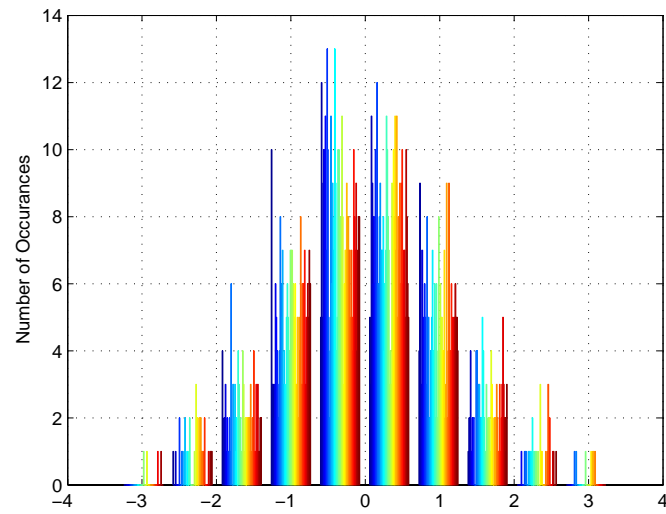


Figure D.1: Histogram of Gaussian Noise Implemented

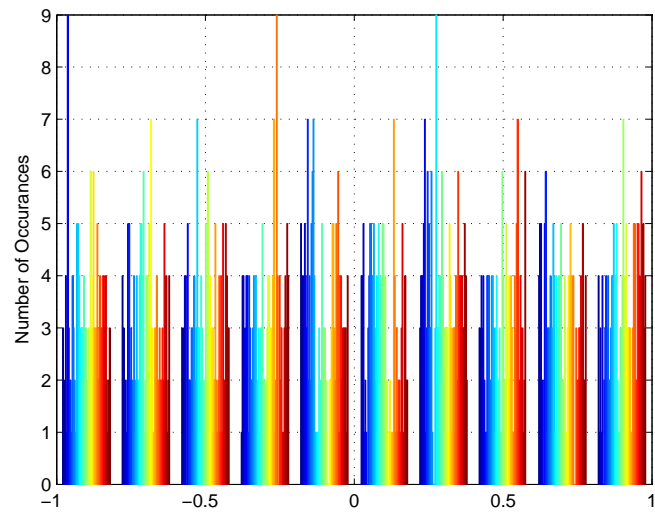


Figure D.2: Histogram of Uniform Noise Implemented

References

- [1] Analog Devices, Inc., One Technology Way, P.O. Box 9106, Norwood, MA 02062-9106, U.S.A. *ADXL202E Hardware and Specification Manual*, REV. A edition, 2000.
- [2] Arch Rock. <http://www.archrock.com>. Website, April 2006.
- [3] Paul E. Black. Lm distance. *Dictionary of Algorithms and Data Structures*, 2004. NIST.
- [4] J. Caffrey, R. Govindan, E. A. Johnson, B. Krishnamachari, S. Masri, G. Sukhatme, K. K. Chintalapudi, K. Dantu, S. Rangwala, A. Sridharan, N. Xu, and M. Zuniga. Networked sensing for structural health monitoring. In *Proceedings of the 4th International Workshop on Structural Control*, 2004.
- [5] P. Cawley and R. D. Adams. The localization of defects in structures from measurements of natural frequencies. *Journal of Strain Analysis*, 14:49–57, 1979.
- [6] E. H. Clayton, B. Koh, G. Xing, L. Fok, S. J. Dyke, and C. Lu. Damage detection and correlation-based localisation using wireless sensor mote sensors. In *Proceedings of the 13th Mediterranean Conference on Control and Automation*, 2005.
- [7] E. H. Clayton, Y. Qian, O. Orjih, S. J. Dyke, A. Mita, and C. Lu. Off-the-shelf modal analysis: Structural health monitoring with motes. In *Proceedings of the 24th International Modal Analysis Conference*, 2006.
- [8] E. H. Clayton and B. F. Spencer. Development of an experimental model for the study of infrastructure preservation. In *Proceedings of the National Conference on Undergraduate Research (NCUR)*, 2002.
- [9] T. Contursi, A. Messina, and E. J. Williams. A multiple-damage location assurance criterion based on natural frequency changes. *Journal of Vibration and Control*, (4):619–633, 1998.
- [10] Crossbow Technology, Inc., 4145 N. First Street, San Jose, CA 95134, U.S.A. *Mica2 Datasheet*, REV. C edition, 2005.
- [11] Crossbow Technology, Inc., 4145 N. First Street, San Jose, CA 95134, U.S.A. *MPR/MIB Users Manual*, REV. B edition, 2005.

- [12] Crossbow Technology, Inc., 4145 N. First Street, San Jose, CA 95134, U.S.A. *MicaZ Datasheet*, REV. A edition, 2006.
- [13] DARPA. <http://www.darpa.mil>. Website, April 2006.
- [14] DARPA. <http://www.darpa.mil/mto/mems/summaries.html>. Website, April 2006.
- [15] F. M. Discenzo, K. A. Loparo, H. Cassar, and D. Chung. Machinery condition monitoring using wireless self-powered sensor nodes. In *Proceedings of the 24th International Modal Analysis Conference (IMAC-XXIV)*, January 2006.
- [16] S. W. Doebling and C. R. Farrar. Statistical damage identification techniques applied to the I-40 bridge over the rio grande river. In *Proceedings of the 16th International Modal Analysis Conference (IMAC-XVI)*, pages 1717–1724, February 1998.
- [17] S. W. Doebling, C. R. Farrar, M. B. Prime, and D. W. Shevitz. Damage identification and health monitoring of structural and mechanical systems from changes in their vibration characteristics: A literature review. Technical Report LA-13070-MS, Los Alamos National Laboratory, May 1996.
- [18] R. O. Duda, P. E. Hart, and D. G. Stork. *Pattern Classification*. John Wiley and Sons, 2nd edition, 2001.
- [19] C. R. Farrar, W. E. Baker, T. M. Bell, K. M. Kone, T. W. Darling, T. A. Duffy, A. Eklund, and A. Migliori. Dynamic characterization and damage detection in the i-40 bridge over the rio grande. Technical Report LA-12767-MS, Los Alamos National Laboratory, June 1994.
- [20] C. R. Farrar and H. Condition/damage monitoring methodologies. In *The Consortium of Organizations for Strong Motion Observation Systems (COSMOS) Workshop*, number LA-UR-01-6573, 2001.
- [21] Yong Gao. *Structural Health Monitoring Strategies for Smart Sensor Networks*. PhD thesis, University of Illinois, Urbana-Champaign, 2005.
- [22] D. Gay, P. Levis, R. Behren, M. Welsh, E. Brewer, and D. Culler. The NesC language: a holistic approach to networked embedded systems. In *Proceedings of the Programming Language Design and Implementation (PLDI)*, June 2003.
- [23] S. D. Glaser. Some real-world applications of wireless sensor nodes. In *Proceedings of the SPIE Symposium on Smart Structures and NDE*, March 2004.

- [24] Marc S. Grunert. Routine uses of NDE applications in Nevada DOT bridge inspection program. In *Proceedings of the 5th ITI Bridge NDE Users Group Conference*. California Department of Transportation Northwestern University Infrastructure Technology Institute, September 1997.
- [25] J. Hill, R. Szewczyk, A. Woo, S. Hollar, D. Culler, and K. Pister. System architecture directions for networked sensors. *Architectural Support for Programming Languages and Operating Systems*, pages 93–1004, 2000.
- [26] B. F. Spencer Jr., M. R. Sandoval, and N. Kurata. Smart sensing technology: Opportunities and challenges. *Journal of Structural Control and Health Monitoring*, 11(4):349–368, September 2004. DOI: 10.1002/stc.48.
- [27] J. N. Juang and R. S. Pappa. An eigensystem realization algorithm for modal parameter identification and modal reduction. *Journal of Guidance, Control and Dynamics*, 8:620–627, 1985.
- [28] B. H. Koh and S. J. Dyke. Structural damage detection in cable-stayed bridges using correlation and sensitivity of modal data. In *The 5th International Workshop Structural Health Monitoring*, page 1234, September 2005.
- [29] H. F. Lam, K. V. Yuen, and J. L. Beck. Structural health monitoring via measured ritz vectors utilizing artificial neural networks. *Computer-Aided Civil and Infrastructure Engineering*, 21(4):232–241, May 2006.
- [30] E. C. Levy. Complex-curve fitting. *IRE Transactions on Automatic Control*, 4:37–44, 1959.
- [31] J. S. Lew. Using transfer function parameter changes for damage detection of structures. *American Institute of Aeronautics and Astronautics Journal*, 33(11):2189–2193, 1995.
- [32] J. P. Lynch. Overview of wireless sensors for real-time health monitoring of civil structures. In *Proceedings of the 4th International Workshop on Structural Control*, pages 189–194, June 2004.
- [33] J. P. Lynch and K. J. Loh. A summary review of wireless sensors and sensor networks for structural health monitoring. *The Shock and Vibration Digest*, 38(2):91–128, 2006.
- [34] J. P. Lynch, A. Sundararajan, H. K. Law, A. S. Kiremidjian, and E. Carryer. Embedding damage detection algorithms in a wireless sensing unit for operational power efficiency. *Smart Materials and Structures*, 13(4):800–810, 2004.
- [35] J. P. Lynch, A. Sundararajan, H. K. Law, H. Sohn, and C. R. Farrar. Piezoelectric structural excitation using a wireless active sensing unit. In *Proceedings of the 22nd International Modal Analysis Conference (IMAC XXII)*, 2004.

- [36] J. P. Lynch, Y. Wang, K. J. Loh, J. H. Yi, and C. B. Yun. Wireless structural monitoring of the geumdang bridge using resolution enhancing signal conditioning. In *Proceedings of the 24th International Modal Analysis Conference (IMAC-XXIV)*, January 2006.
- [37] MEMS Net. <http://www.memsnet.org>. Website, August 2005.
- [38] A. Messina, I. A. Jones, and E. J. Williams. Damage detection and localization using natural frequency changes. In *Proceedings of the Conference on Identification in Engineering Systems*, pages 67–76, 1996.
- [39] A. Messina, E. J. Williams, and T. Contursi. Structural damage detection by a sensitivity and statistical-based method. *Journal of Sound and Vibration*, 216(5):619–633, 1998.
- [40] K. Mitchell, S. Sana, Balakrishnan V. S., V. S. Rao, and H. J. Pottinger. Micro sensors for health monitoring of smart structures. In *Proceedings of the SPIE Conference on Smart Electronics and MEMS*, volume 3673, pages 315–358. SPIE, March 1999.
- [41] T. Nagayama, M. Ruiz-Sandoval, B. F. Spencer Jr., K. A. Mechitov, and G. Agha. Wireless strain sensor development for civil infrastructure. In *Proceedings of the First International Workshop on Networked Sensing Systems*, pages 97–100, 2004.
- [42] A History of Porcelain. <http://www.artistictile.net/frameset> Website, March 2006.
- [43] American Institute of Steel Construction. *Load Resistance Factor Design Manual*. American Institute of Steel Construction, One East Wacker Drive Suite 700, Chicago, IL 60601, 3 edition, November 2001.
- [44] J. Paek, K. K. Chintalapudi, J. Caffrey, R. Govindan, and S. Masri. A wireless sensor network for structural health monitoring: Performance and experience. In *Proceedings of the 2nd IEEE Workshop for Embedded Networked Sensors (EMNETS)*, pages 13–24, 2005.
- [45] S. N. Pakzad and G. L. Fenves. Structural health monitoring applications using MEMS sensor networks. In *Proceedings of the 4th International Workshop on Structural Control*, 2004.
- [46] D. J. Pines and P. A. Lovell. Conceptual framework of a remote wireless health monitoring system for large civil structures. *Journal of Smart Materials and Structures*, 7(5):627–636, 1998. DOI:10.1088/0964-1726/7/5/007.

- [47] J. Polastre, J. Hill, and D. Culler. Versatile low power media access for wireless sensor networks. In *Proceedings of the 2nd ACM Conference on Embedded Networked Sensor Systems (SenSys'04)*, 2004.
- [48] Y. Qian, A. Mita, E. H. Clayton, and S. J. Dyke. Experimental study on localization and quantification of structural damage using zigbee motes. In *Third European Workshop on Structural Health Monitoring*, July 2006.
- [49] Manuel E. Ruiz-Sandoval. *Smart Sensors for Civil Engineering Infrastructure Systems*. PhD thesis, University of Notre Dame, May 2004.
- [50] Anders Rytter. *Vibrational Based Inspection of Civil Engineering Structures*. PhD thesis, University of Aalborg, April 1993.
- [51] Sir A. Schuster. On the investigation of hidden periodicities with application to a supposed twenty-six day period of meteorological phenomena. *Terrestrial Magnetism*, 3(13):lookup, 1898.
- [52] V. Shnayder, M. Hempstead, B. Chen, G. Werner-Allen, and Matt Welsh. Simulating the power consumption of large-scale sensor network applications. In *Proceedings of the Second ACM Conference on Embedded Networked Sensor Systems (SenSys'04)*, November 2004.
- [53] H. Sohn, C. R. Farrar, D. D. Shunk, D. W. Stinemates, B. R. Nadler, and J. J. Czarnecki. A review of structural health monitoring literature: 1996–2001. Technical Report LA-13976-MS, Los Alamos National Laboratory, 2004.
- [54] The Math Works Inc. *Signal Processing Toolbox Users Guide*. Math Works Inc., 1998.
- [55] TinyOS. <http://webs.cs.berkeley.edu/tos>. Website, June 2005.
- [56] M. W. Vanik, J. L. Beck, and S. K. Au. Bayesian probabilistic approach to structural health monitoring. *Journal of Engineering Mechanics*, 126(7):738–745, 2000.
- [57] Webopedia. <http://www.webopedia.com>. Website, 2006.
- [58] Wikipedia. <http://www.wikipedia.org>. Website, 2006.
- [59] N. Xu, S. Rangwala, K. K. Chintalapudi, D. Ganesan, A. Broad, and D. Estrin. A wireless sensor network for structural health monitoring. In *Proceedings of the 2nd ACM Conference on Embedded Networked Sensor Systems (SenSys'04)*, 2004.

- [60] R. J. Zhang, W. Q. Wang, S. H. Hou, and C. K. Chan. Modal analysis for beam bundle in fluid. *Journal of Pressure Vessel Technology*, 124(2):223–228, May 2002. DOI: 10.1115/1.1427341.
- [61] J. Zhao and R. Govidan. Understanding packet delivery performance in dense wireless sensor networks. In *Proceedings of the 1st ACM Conference on Embedded Networked Sensor Systems (SenSys'03)*, 2003.

Vita

Erik H. Clayton

Date of Birth	July 29, 1979
Place of Birth	Grand Rapids, Michigan
Degrees	B.S. Summa Cum Laude, Civil Engineering, May 2003 M.S. Civil Engineering, May 2006
Awards	GAANN Graduate Fellowship Recipient <i>Washington University in St. Louis, (2004–2006)</i> D.J. DeMichele Scholarship Recipient <i>International Modal Analysis Conference XXIV (2006)</i> Helwig Graduate Fellowship Recipient <i>California Institute of Technology, (2003–2004)</i> Special Institute Graduate Fellowship Recipient <i>California Institute of Technology, (2003–2004)</i> Callaway, Duggan, and AASHTO Scholarship Recipient <i>University of Tennessee, (2001–2003)</i>
Academic Experience	<i>Graduate Research Assistant</i> Washington University in St. Louis (2004–Present) <i>Instructor</i> CE336 Engineering Materials Laboratory Washington University in St. Louis (F2004, F2005) <i>Substitute Instructor</i> CE550 Advance Structural Dynamics Washington University in St. Louis (F2005) <i>Visiting Graduate Research Assistant</i> Keio University (2005)

Graduate Student

California Institute of Technology (2003-2004)

*Undergraduate Research Assistant*Washington University in St. Louis and University of Tokyo
(S2002)*Undergraduate Research Assistant*

University of Tennessee (2001-2002)

Undergraduate Research Assistant

University of Notre Dame (S2001)

Industry*Senior Engineering Assistant***Experience**

ATA Engineering, Inc. , San Diego, CA

Structural Engineer Intern

Mallia Engineering Co. , Knoxville, TN

**Professional
Societies**

Society for Experimental Mechanics (SEM)

American Society of Civil Engineers (ASCE)

Earthquake Engineering Research Institute (EERI)

Engineers' Club of St. Louis

Sigma Xi

Tau Beta Pi

Chi Epsilon

Phi Eta Sigma

Publications

Clayton, E. H., Qian, Y., Orjih, O., Dyke, S. J., Mita, A., Lu, C. (2006). "Off-the-Shelf Modal Analysis: Structural Health Monitoring with Motes Monitoring", *Proceedings of the 24th International Modal Analysis Conference (IMAC XXIV)*.

Song, W., Giraldo, D. F., Clayton, E. H., Dyke, S. J., Ciacedo, J. M. (2006). "Application of ARMAV for Modal Identification of the Emerson Bridge", *Proceedings of the Third International Conference on Bridge Maintenance, Safety and Management (IABMAS06)*.

Qian, Y., Mita, A. Clayton, E. H., Dyke, S. J. (2006). "Experimental study on localization and quantification of structural

damage using ZigBee Motes”, *Proceedings of the Third European Workshop on Structural Health Monitoring*.

Clayton, E. H., Koh, B. H., Xing, G., Fok, C. L., Dyke, S. J., Lu, C. (2005). “Damage Detection and Correlation-based Localization Using Wireless Mote Sensors”, *Proceedings of the 13th Mediterranean Conference on Control and Automation (MED05)*.

Caicedo, J M., Clayton, E. H., Dyke, S. J., Abe, M. (2002). “Structural Health Monitoring for Large Structures Using Ambient Vibrations”, *Proceedings of The International Conference on Advances and New Challenges in Earthquake Engineering Research (ICANCEER)*.

Clayton, E. H., Spencer, B. F., Jr. (2001). “Development of an Experimental Model for the Study of Infrastructure Preservation”, *Proceedings of the National Conference on Undergraduate Research (NCUR)*.

May 2006

Short Title: SHM with Smart Wireless Sensors

Clayton, M.S. 2006